Award Title: Fusion-Enabled Pluto Orbiter and Lander
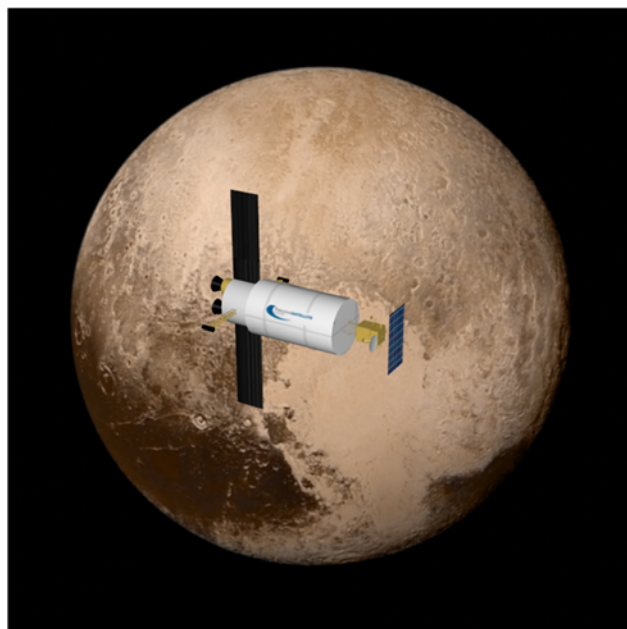
Report Type: Phase I Final Report

Principal Investigator: Ms. Stephanie Thomas

Period of Performance: May 13, 2016 through May 12, 2017

Institution: Princeton Satellite Systems, Inc.
6 Market St. Suite 926
Plainsboro, NJ 08536

Award Number: NNX16AK28G

Executive Summary

The Pluto orbiter mission proposed here is credible and exciting. The benefits to this and all outer-planet and interstellar-probe missions are difficult to overstate. The enabling technology, Direct Fusion Drive, is a unique fusion engine concept based on the Princeton Field-Reversed Configuration (PFRC) fusion reactor under development at the Princeton Plasma Physics Laboratory. The truly game-changing levels of thrust and power in a modestly sized package could integrate with our current launch infrastructure while radically expanding the science capability of these missions.

During this Phase I effort, we made great strides in modeling the engine efficiency, thrust, and specific impulse and analyzing feasible trajectories. Based on 2D fluid modeling of the fusion reactor's outer stratum, its scrape-off-layer (SOL), we estimate achieving 2.5 to 5 N of thrust for each megawatt of fusion power, reaching a specific impulse, Isp, of about 10,000 s. Supporting this model are particle-in-cell calculations of energy transfer from the fusion products to the SOL electrons. Subsequently, this energy is transferred to the ions as they expand through the magnetic nozzle and beyond.

Our point solution for the Pluto mission now delivers 1000 kg of payload to Pluto orbit in 3.75 years using 7.5 N constant thrust. This could potentially be achieved with a single 1 MW engine. The departure spiral from Earth orbit and insertion spiral to Pluto orbit require only a small portion of the total delta-V. Departing from low Earth orbit reduces mission cost while increasing available mission mass. The payload includes a lander, which utilizes a standard green propellant engine for the landing sequence. The lander has about 4 square meters of solar panels mounted on a gimbal that allows it to track the orbiter, which beams 30 to 50 kW of power using a 1080 nm laser. Optical communication provides dramatically high data rates back to Earth.

Our mass modeling investigations revealed that if current high-temperature superconductors are utilized at liquid nitrogen temperatures, they drive the mass of the engine, partly because of the shielding required to maintain their critical temperature. Second generation materials are thinner but the superconductor is a very thin layer deposited on a substrate with additional layers of metallic classing. Tremendous research is being performed on a variety of these superconducting materials, and new irradiation data is now available. This raises the possibility of operating near-future "high-temperature" superconductors at a moderately low temperature to dramatically reduce the amount of shielding required. At the same time, a first generation space engine may require low-temperature superconductors, which are higher TRL and have been designed for space coils before (AMS-02 experiment for the ISS).

We performed detailed analysis of the startup system and thermal conversion system components. The ideal working fluid was determined to be a blend of Helium and Xenon. No significant problems were identified with these subsystems. For the RF system, we conceived of a new, more efficient design using state-of-the-art switch amplifiers, which have the potential for 100% efficiency.

This report presents details of our engine and trajectory analyses, mass modeling efforts, and updated vehicle designs.

<u>Table of contents</u>

List of Figures

List of Tables

1 Introduction

The Pluto orbiter mission proposed here is credible and exciting. The benefits to this and all robotic outer planet or manned interplanetary missions are difficult to overstate. The enabling technology, Direct Fusion Drive, is a unique fusion engine concept based on the Princeton Field-Reversed Configuration (PFRC) fusion reactor under development at the Princeton Plasma Physics Laboratory. The truly game-changing levels of thrust and power in a modestly sized package could integrate with our current launch infrastructure while radically expanding the science capability of these missions. Figure 1 shows an artistic rendition of the space reactor, with key components labeled.
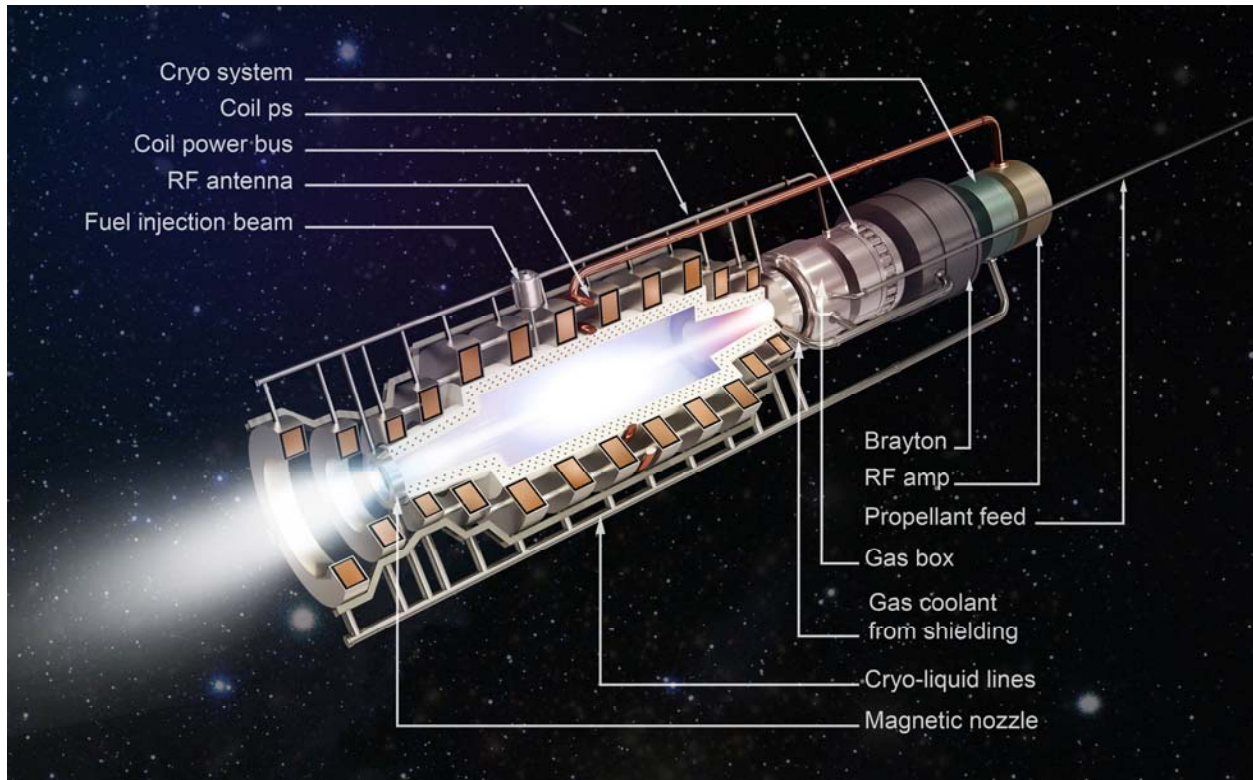
Figure 1. Artistic rendering of the DFD engine with an interior cutout to show detail of the coils.

The mission context we have proposed is delivery of a Pluto orbiter with a lander. Direct Fusion Drive (DFD) provides high thrust to allow for reasonable transit times to Pluto while delivering substantial mass to orbit: 1000 kg delivered in under four years using 5-10 N thrust.

Since DFD provides power as well as propulsion in one integrated device, it will also provide as much as 2 MW of power to the payloads upon arrival. This enables high-bandwidth communication, powering of the lander from orbit, and radically expanded options for instrument design. The data acquired by New Horizons' recent Pluto flyby are just a tiny fraction of the scientific data that could be generated from an orbiter and lander.

To date our work on the space applications and balance-of-plant has been entirely funded by internal research and development. Our work has included preliminary analysis of a variety of space missions, from outer planets missions to asteroid deflection to interstellar missions, but

funding levels have precluded detailed subsystems analysis. Our computations show that the predicted thrust level can accomplish the mission and that no other plausible technology can deliver such significant mass and power-producing capability to Pluto orbit with a flight duration of just a few years and relatively low development and launch costs.

2 Methods and Assumptions

2.1 Work Plan

In this Phase I study, we proposed to analyze the Pluto mission concept using new models of the predicted DFD engine characteristics. The goal is to determine the feasibility of the preliminary trajectory concept by applying limits on the thrust steering and range of throttle. The throttling of the thrust and specific impulse will affect the efficiency. We subcontracted to Princeton Plasma Physics Laboratory for part of this investigation. The subtasks are:

1. Analyze all subsystems and produce an improved mass model
2. Analyze shielding requirements on a component level and produce an improved shielding design and neutron radiation mitigation strategy
3. Analyze the thrust augmentation system and produce a model of efficiency vs. thrust (subcontract to Princeton Plasma Physic Lab)
4. Using the new mass and thrust models generate an optimal Pluto mission trajectory
5. Revisit the system design and produce a new spacecraft model

Figure 2 shows a block diagram of the system components. The blocks that we are studying in this Phase I project are shaded light blue. In Phase I we have not performed any analysis of the superconducting coil cooling subsystem, but have focused on the heat engine, startup system, and the RF generator.
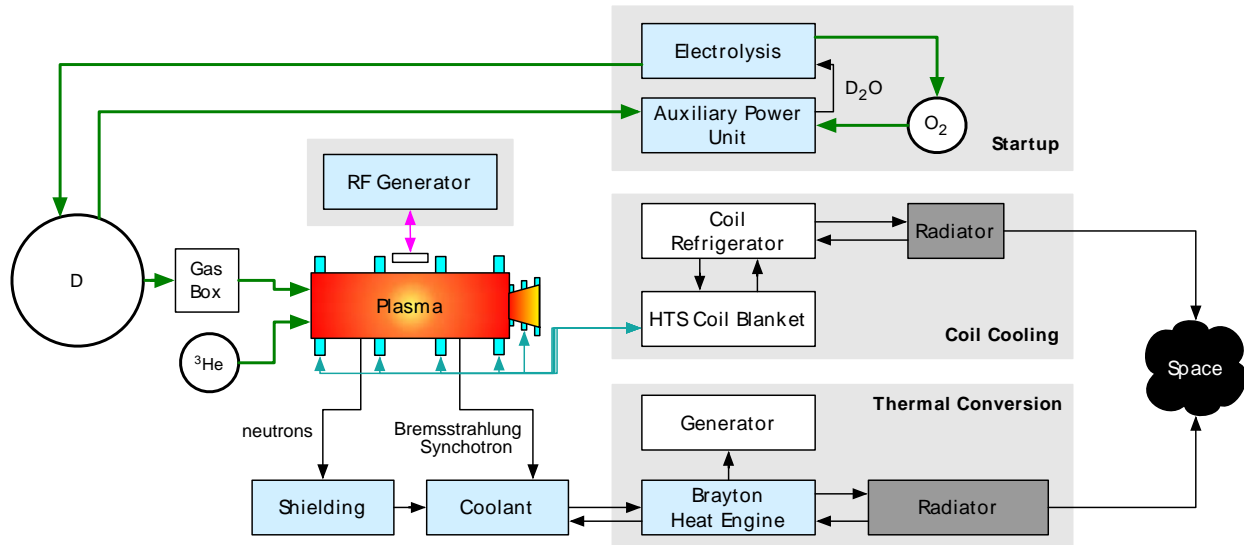
Figure 2. DFD System Components. Our Phase I focused on analysis of the components shaded in blue.

Approximately 550 hours were allocated to PSS staff for the modeling and system analysis and 80 hours for PPPL's Dr. Cohen to develop a model of the thrust augmentation system that evaluates engine efficiency, thrust, and specific impulse.

2.2 Princeton Field-Reversed Configuration (PFRC) Reactor

The Direct Fusion Drive concept is an extension of ongoing fusion research at Princeton Plasma Physics Laboratory dating to 2002. Princeton Field-Reversed Configuration machines (PFRC) employ a unique radio frequency (RF) heating method invented by Dr. Samuel Cohen. Studies of electron heating with this method have surpassed theoretical predictions and experiments to measure ion heating in the second-generation machine are ongoing.

A full-sized PFRC is perfectly suited to use as a rocket engine for two reasons: one, the configuration results in a radical reduction of neutron production compared to other D^3-He approaches; two, the reactor features an axial flow of cool plasma to absorb the energy of the fusion products. Adding propellant to this flow results in a variable thrust, variable specific impulse exhaust through a magnetic nozzle. We call this process *thrust augmentation* of the reactor. Approximately 35% of the fusion power goes to thrust, 30% to electric power, 25% lost to heat, and 10% is recirculated for the RF heating.

The current one-quarter-scale machine, the PFRC-2 with a plasma radius to 7 cm (see Figure 3), is designed to demonstrate electron and ion heating. At an applied RF heating power of about 20 kW, electron heating to temperatures $T_e > 300$ eV has been demonstrated, see Figure 4. Ion heating studies will follow, once $T_e > 1$ keV has been achieved. Pulse lengths of 300 ms have been reached. The main axial-field water-cooled magnets, in conjunction with eight high-temperature superconducting internal flux conservers can produce a central internal field of 1.2 kG. (An operational PFRC would have a field of 70 kG). The RF heating system has been upgraded to 200 kW. Additional diagnostics have been added, a notable one being a soft X-ray pulse-height spectrometer with an spectral range of 0.25-10 keV, an energy resolution of 9% at

525 eV and 1% at 5.9 keV, and a count rate capability to in excess of 10^6/s. Probes are used to measure SOL properties.
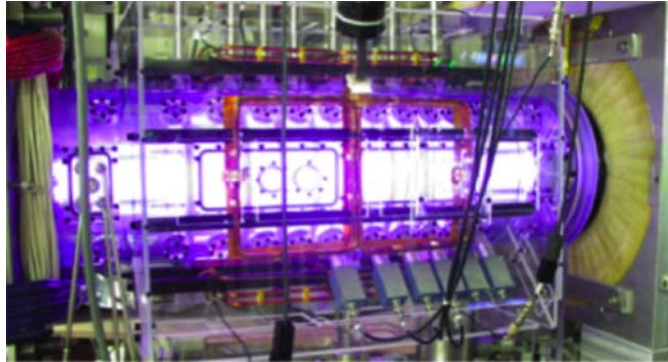
Figure 3. PFRC-2 in operation. This photo captures a pulse; the plasma is white inside a Lexan vacuum vessel. An external RF antenna can be seen as Kapton-tape wrapped square figure-8's. [Courtsey C. Swanson and P. Jandovitz]
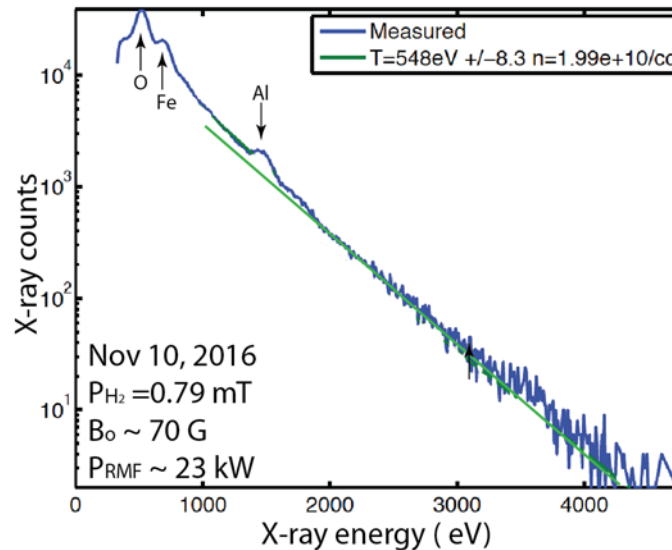
Figure 4. X-ray spectrum from a recent PFRC-2 RMF run. The tail electron temperature reached over 500 eV and the bulk temperature over 300 eV.

2.3 Modeling Tools

2.3.1 Plasma Software Packages
There are four main software packages that have been used to analyze the PFRC configuration and operation:

1. LSP - This is a 3-D electromagnetic particle-in-cell code for Large Scale Plasma simulations. This is commercial software owned by Orbital/ATK and run under a PPPL license. This code has been used to study FRC formation by RMF, RMF penetration, plasma heating, and fast-ion slowing down in cool magnetized plasmas. It requires significant supercomputer time, typically 10^5 cpu-hrs per run.

2. UEDGE - This 2-D multi-species fluid code predicts electron and ion temperatures based on a specified magnetic configuration and plasma, neutral gas, and power input. Lawrence Livermore National Lab staff wrote and maintain this code.[1]

3. RMF - This Hamiltonian code, authored by Alan Glasser, models single-particle heating in 3-D with specified magnetic fields, *e.g.*, FRCs and RMF.

4. ATTILA – a comprehensive radiation transport environment. This code is used to model radiation effects in ITER, including neutron transport, activation, and defect generation.

ATTILA was used in prior work to generate shielding thicknesses based on certain neutron power and acceptable neutron fluences. UEDGE was used during the course of this study to generate new simulation results for thrust and specific impulse as a function of input power and gas flow rate. RMF and LSP have been used in prior work to build the theoretical foundation of PFRC operation including detachment in the terminating magnetic nozzle. For more details see Appendix A which has a detailed technical description of the PFRC.

2.3.2 Spacecraft Control Toolbox: Fusion Propulsion Module

This software packaged was initially developed using internal research and development funds. It includes the following tools:
*   plasma physics utilities
*   fusion reactions including the power released by each species and cross-sections
*   Bremsstrahlung and synchrotron radiation models
*   magnet sizing using Virial and shell methods
*   power conversion system sizing (L. S. Mason 2003)
*   tools for sizing shielding and cryogenic cooling systems
*   point reactor designs (Santarius 1998)
*   rectilinear mission planning

During this Phase I, we added additional plasma models from the 2016 NRL Plasma Formulary, as well as additional fusion cross-section models. (Hively 1982)

3 Results

3.1 Mass Model

The goal of this task was to develop detailed tables of the mass and power numbers for a complete DFD system as to better estimate the specific power of the technology. Previous estimates have used mass scaling laws, such as for a gas turbine. We want to move away from scaling laws and size the individual components in the heat exchanger, RF system, and radiators,

---

[1] (T.D. Rognlien, 2000)

as well as the support structure for the coils. We also began analysis of layout options and developed an initial layout in a CAD package.

The following subsections report on each subsystem analyzed and the final subsection provides the component mass tables.

3.1.1 Thermal Conversion

A Rankine cycle was eliminated from consideration because it has a lower technological maturity and higher operational complexity than the other two. In spaceflight applications, reducing complexity is an important design parameter. The reason that a Brayton cycle was chosen over a Stirling cycle is because of its projected operational efficiency. For low-power, nuclear-based space plants, Stirling engines offer a significantly lower system mass than Brayton engines. However, at power levels greater than 20 kW, Brayton engines begin to become more efficient in terms of mass-to-power-output levels (L. Mason 2002). As this spacecraft is operating in the MW range, a Brayton cycle is the clear choice.

Figure 5 shows a basic Brayton cycle with a recuperator. The components of a Brayton Cycle are:
1. Compressor 1 - a low pressure compressor
2. Intercooler - cools the gas before entering the next compressor stage. It cools by passing the gas over the radiator, which rejects heat to space.
3. Compressor 2 - a high pressure compressor
4. Recuperator - a primary heat exchanger that heats gas coming from the compressor prior to heat addition by the external source. This increases efficiency by raising the temperature seen at the turbine. However, if the external source already heats the working fluid to the turbine blade limit of 1589 K, a recuperator may not be needed.
5. Heat source - heat from the fusion engine is transferred into the cooling loops that house the working fluid via radiation.
6. Turbine 1 - a low pressure turbine
7. Turbine 2 - a high pressure turbine
8. Generator - converts turbine work output into electrical energy for use by the rest of the spacecraft
9. Precooler - transfers heat to the radiators in order to cool the working fluid down to an acceptable level to be fed into the first compressor
10. Radiator - rejects waste heat to space

The turbine and compressor can have any number of stages: only two are shown here. Notice in the figure that the compressors are connected with a shaft to Turbine 1, which is how they receive their power. Similarly, the generator is connected to Turbine 2, which is how the electrical energy for the spacecraft is generated. Excluding preheaters in-between turbine stages, this list contains all of the possible components in a closed loop Brayton cycle. However, it is likely that not every component will be used in the actual system.
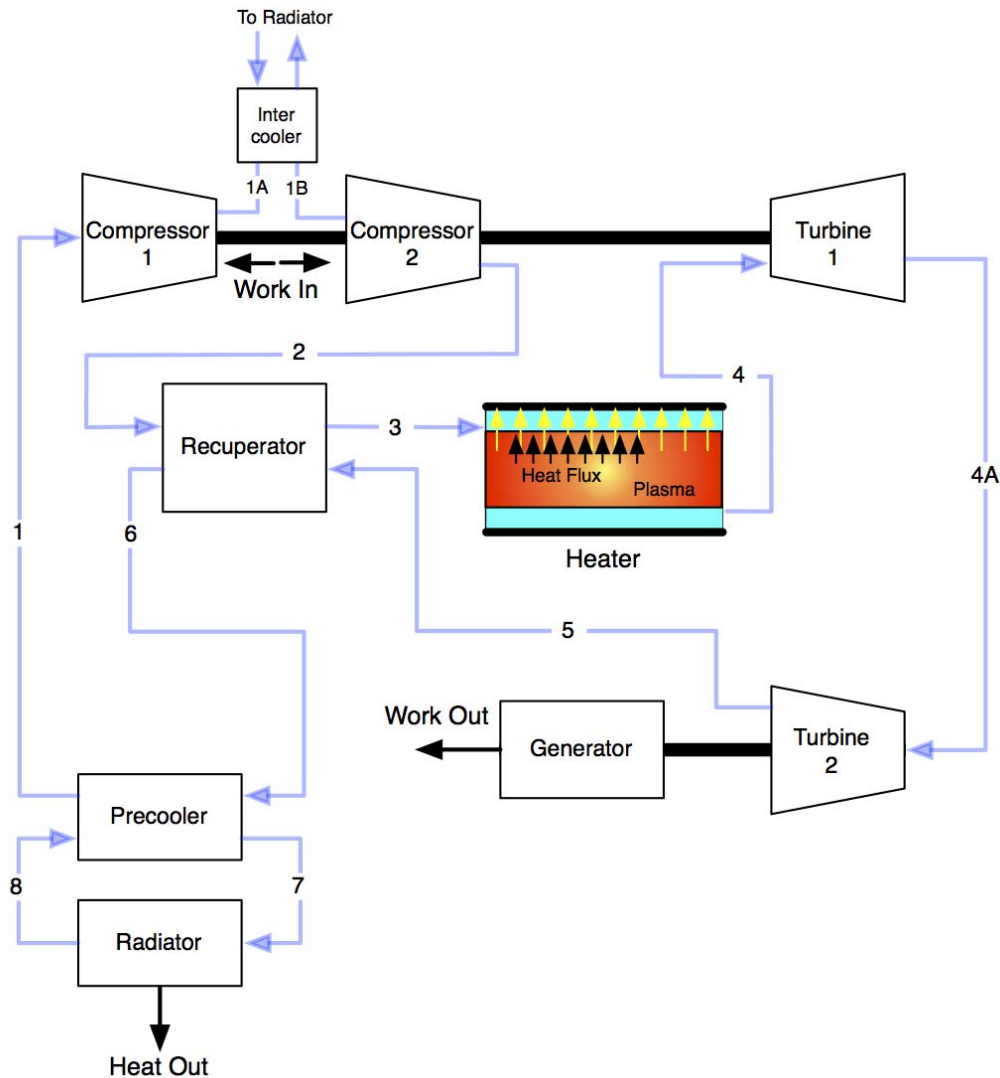
Figure 5. Brayton Cycle with Recuperator.

In Figure 5, the working fluid first enters Compressor 1. The compressor is driven by Turbine 1, though it will need power at the start of the cycle from elsewhere. This will come from the D2/O2 combustion that also powers the start-up of the Heater. The fluid's pressure and temperature increase as it passes through Compressor 1. In order to maximize efficiency of subsequent compressors, the fluid will be cooled before entering each one. After exiting the last compressor, it may be passed through a Recuperator in order to be pre-heated. This depends on the mission's operating parameters and the power dissipation of the Heater. After the Recuperator, the working fluid will pass into cooling coils that loop around the nuclear reactor.

At this point, the working fluid will be heated to very high temperatures - around 1500 K - through radiation absorption. This hot fluid will then be passed through a series of turbines in order to generate power. The compressors will be directly driven by turbines, and the turbines that remain at the end of the series will be used to drive an electricity-producing generator. After passing out of the turbines, the gas will have cooled but will still be relatively hot. It also will have dropped to roughly the same pressure as the inlet stream to Compressor 1. The gas may pass through a Recuperator to further cool it before being passed into the pre-cooler heat exchanger to bring it down to its original temperature.

This is how the Brayton cycle works: fluid is compressed, heated, passed through turbines to generate power, and then cooled. Whereas jet engines employ open-loop Brayton cycles using air as the working fluid, all space applications must employ the closed-loop version to contain the working fluid.

Two MATLAB codes, one with and one without a recuperator, have been developed to accurately model a non-ideal closed-loop Brayton Cycle. The scripts take an inlet pressure, inlet temperature, and desired pressure ratio as inputs, and calculate pressure, temperature, flow rate, cycle efficiency, and work for each step as outputs. Adjustable parameters in the scripts are as follows:
1. Baseline pressure
2. Baseline temperature
3. Pressure ratio
4. Compressor efficiency
5. Turbine efficiency
6. Recuperator effectiveness
7. Working fluid specific heat ratio
8. Working fluid specific heat
9. Working fluid molecular weight

Figure 6 shows sample output for a pressure ratio of 2. The temperature and pressure are noted for each stage. The efficiency is only 20% without the recuperator.
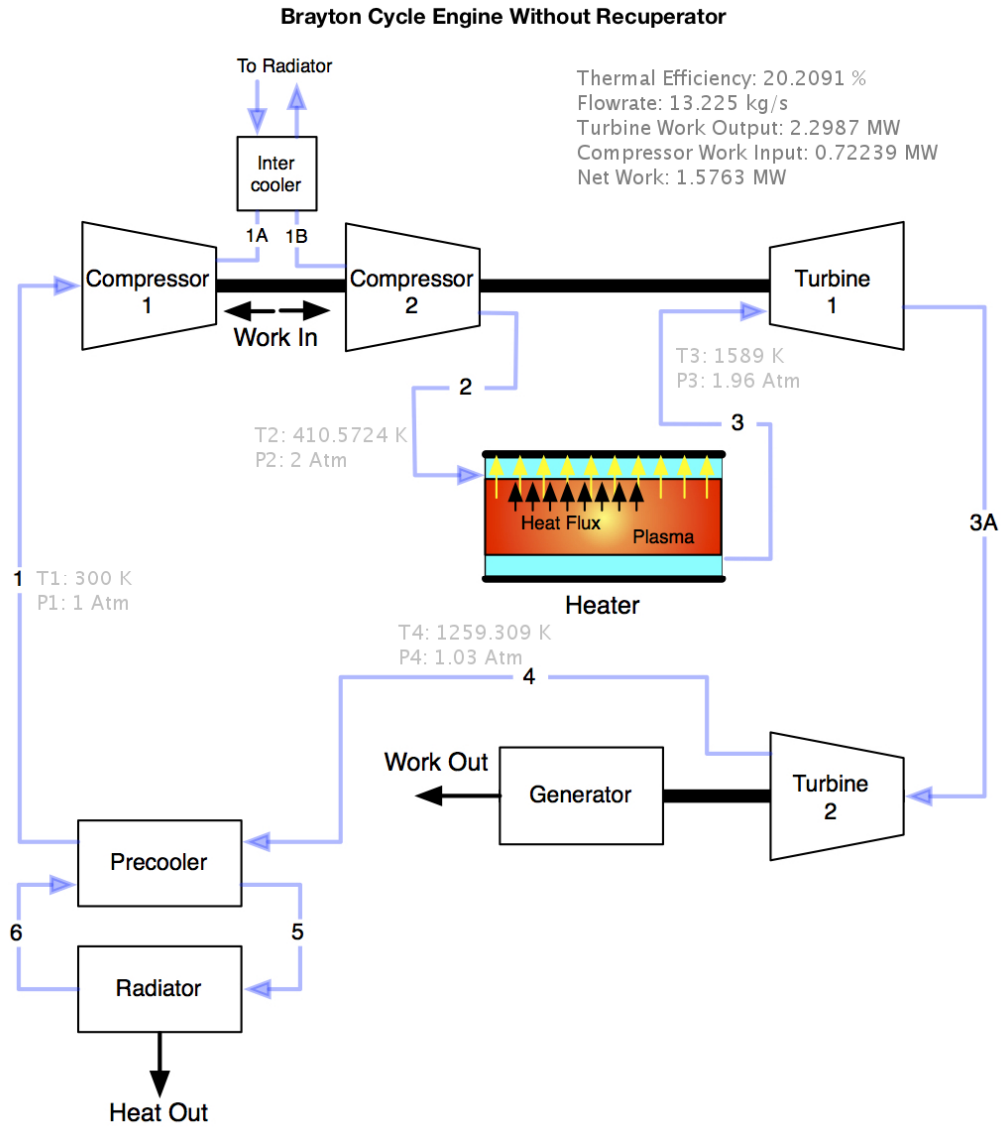
Figure 6. Output of MATLAB Model for the Brayton Cycle
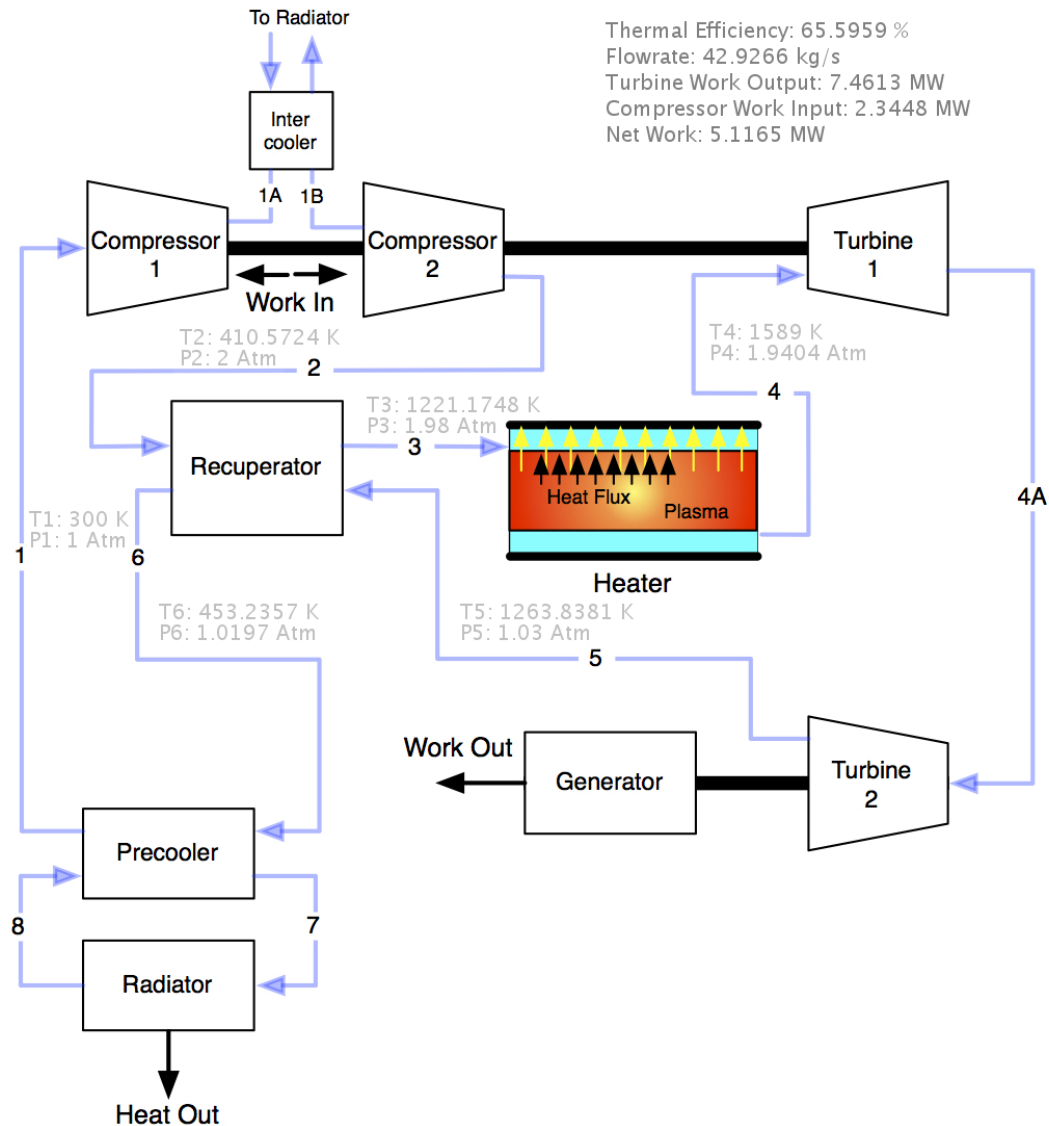
Figure 7. Output of MATLAB Model for the Brayton Cycle with a Recuperator

Several working fluid options have been considered for Brayton Cycles with similar applications to this proposal. Monatomic working fluids of interest include Helium (He), Argon (Ar), and Xenon (Xe). All are noble gases and are thus stable and non-reactive. Diatomic working fluids include Nitrogen (N2) and Hydrogen (H2). Carbon Dioxide (CO2) has been considered as a polyatomic working fluid. Finally, gas mixtures are often considered, including He-Ar and He-Xe.

For this concept, a 70/30 mole fraction mixture of helium and xenon was chosen to be the working fluid. There are a number of reasons why this mixture is advantageous over pure helium or hydrogen:

- The higher molecular weight of the mixture increases both the turbine and compressor efficiencies. Because of its higher molecular weight, Xenon has a lower value of beta, which is derived from its value of (1 – specific heat ratio) . A lower value of beta means that an increase in pressure drop will correspond to a lower change in temperature.

- Higher pressure drops and smaller temperature changes are ideal. Thus, by utilizing a working fluid with a higher molecular weight, the increase in turbine and compressor efficiencies can increase the overall system efficiency up to 50% [Wright et al., 2002].
- The molecular weight of the mixture (42.2g/mol) is closer to that of air (28.8g/mol) than pure helium (4g/mol), making it easier to design and test the turbines and compressors.
- Higher molecular weight working fluids allow the design of turbines of better performance.
- Lower kinematic viscosities result in higher power generation efficiencies [?]. Xenon significantly lowers the kinematic viscosity of the working fluid compared to that of a pure helium system.
- The mixture has been found to reduce the turbine exit impeller-root stress by up to 50% [Klann, 1968]. This increases the lifetime of the system.

One downside to increasing the molecular weight by adding Xenon into the working fluid is that the heat capacity and thermal conductivity decrease. However, the gains in efficiencies and ease of testing outweigh the decrease in thermal control.

Figure 8 shows a schematic layout of the Brayton cycle components relative to the DFD main engine, to help in determining the length of the pipes required between the components. Note the lengths given, which assume that the main engine is 4 m long and 1 m in diameter. There needs to be an intercooler (IC) between each compressor stage (C1, C2, …) This results in a total cycle pipe length of 15 m.
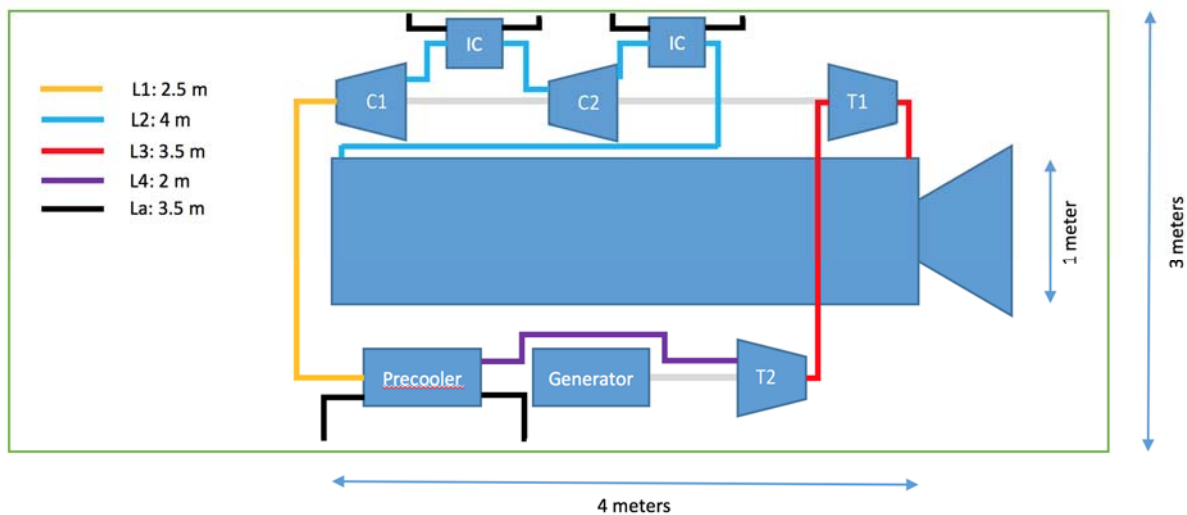
Figure 8. Brayton Engine Component Schematic

Table 1 gives the key design parameters selected for sizing the Brayton cycle.

Table 1. Brayton Engine Design Parameters

Parameter	Value
Working fluid	70/30 molar fraction He-Xe
Input heat	350 kW

Max fluid temperature	1589 K
Compressor stages	6
Pressure ratio	Up to 30
Pipe material	Stainless steel

Table 2 gives estimates for the component masses. The generator mass is based on existing electric vehicle motors, which produce about 150 kW in about 80 kg. The turbine and compressor masses are scaled using GE90 jet engine which uses the same pressure ratio, temperature, and ceramic blade material as our system. The piping assumes 18 cm diameter stainless pipes with a wall thickness of 0.2 cm.

Table 2. Brayton Engine Component Mass Estimates

Component	Mass (kg)
Turbines and Compressors	30 kg
Piping (stainless steel)	130 kg
Generator	80 kg
SUBTOTAL	240 kg

3.1.2 Startup Subsystem

Our startup concept uses combustion of the available deuterium in an auxiliary power unit (APU), which can start up the fusion engine. An oxygen tank is required. An optional electrolysis unit can then recuperate the oxygen for future restarts. The heat from the APU is converted to electricity using the same thermal conversion system as the main engine.
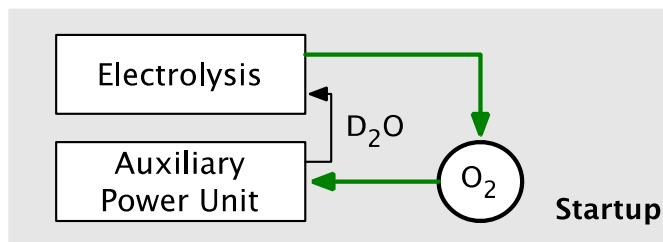
Figure 9. Startup system components.

1 kg Hydrogen produces 120 MJ/kg of energy when combusted with 8 kg of oxygen. Deuterium has double the atomic mass of hydrogen, so twice as much is required, and 2 kg of deuterium produces approximately the same energy. The engine is started up at partial power in electricity generation mode and this power replaces the power from the combustion as the engines return to full power. The combustor uses the same heat engine as the nuclear fusion engine uses for power generation.

The D_2-O_2 Auxilary Power Unit (APU) will therefore be used to generate heat through the combustion of deuterium. This heat will be transported via the gaseous water (steam) outflow from the reaction. The steam will be passed through a heat exchanger in order to transfer the heat to the helium-xenon working fluid in the Brayton cycle. This heat will then reach its final

destination, where the Brayton cycle will convert it to useful energy via a generator. This startup process is shown in Figure 10. When actuated valves are opened electrically from the battery supply, oxygen and deuterium will flow through an injector plate and into the combustion chamber. They will be electrically ignited and combust to form hot steam. This steam will flow through a heat exchanger and transfer its heat to the helium-xenon working fluid. The heat will then be converted to electricity in the Brayton Heat Engine for use in energizing the coils, powering the RF Heater, and charging the battery. Meanwhile, the cooled steam will pass through a condenser to change back to its liquid state so that it can be electrolyzed and fed into the deuterium and oxygen tanks for recycling.
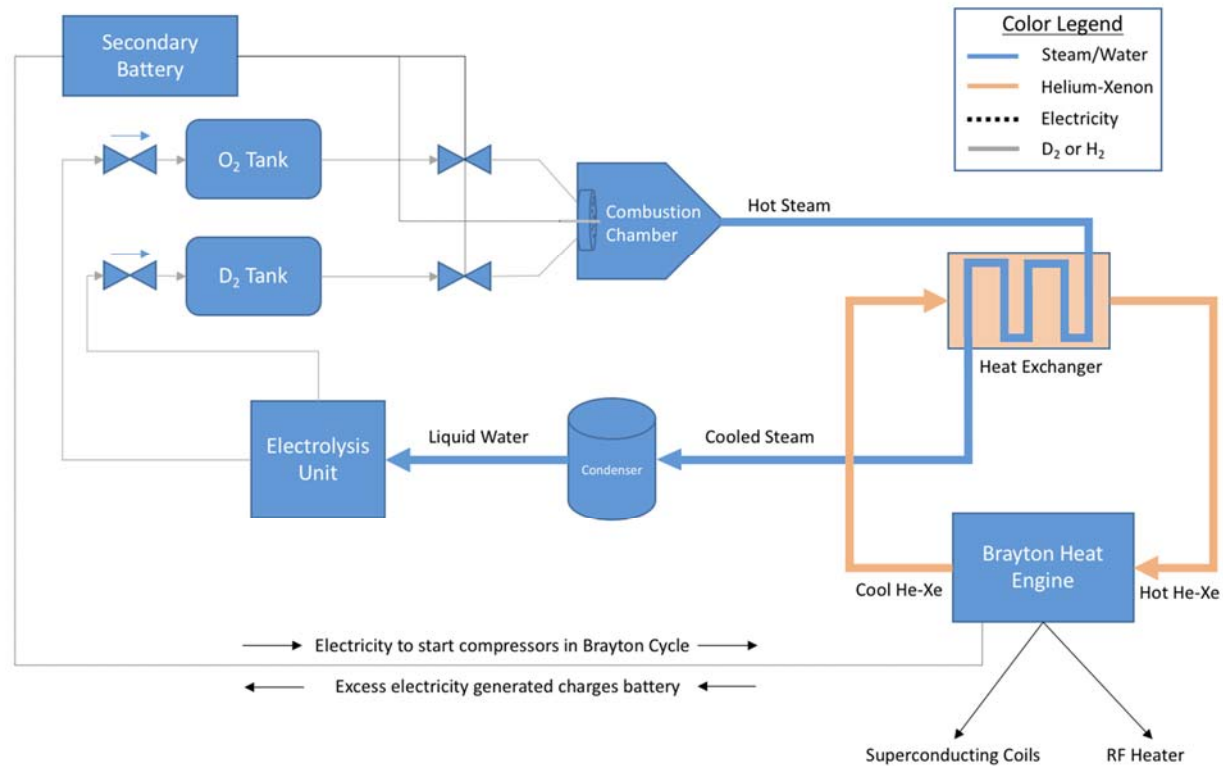
Figure 10. D2O2 APU Startup Block Diagram

We estimate that the startup system should provide about 20% of the full engine power for 1000 seconds. For a 10 MW engine, this is 2 MW for 100 s, or 200 MJ. This will require 13.5 kg oxygen and 3.4 kg deuterium.

For extremely long duration missions, the D_2O can be electrolyzed once the engine has restarted. This provides oxygen for future restarts. On spacecraft with a crew there is likely to be sufficient O_2 for this purpose without the needed for the added mass of an electrolysis unit. The electrolysis unit is sized based on the rate of electrolysis, or how quickly the oxygen needs to be recovered. The ISS unit has a mass of 446 kg and can produce 5 kg of oxygen per day. If we scale down from this system, we might have a unit that is 100 kg if we want to produce 1.5 kg per day or 15 kg if we want to produce 0.135 kg per day, which would require 100 days to regenerate the 13.5 kg oxygen consumed.

The components required in the system are additional valves, the oxygen tank, piping, the combustion chamber, the heat exchanger, the condenser, and optionally, the electrolysis unit. The combustion chamber will require a fuel injector and an igniter plate, similar to a rocket engine. For example, the RL-10B-2 engine produces 249 MW with a total mass of 277 kg; approximately 80 kg of this mass is the combustor unit itself. We can't scale down from this directly, but can assume a 2 MW unit (or less for a 1-5 MW engine) will be a small fraction of this. The shell in tube heat exchanger is comprised of a bundle of pipes. If 40 1" diameter aluminum pipes are used, and the unit is 24" long, the mass of the tubes is about 6 kg and the enclosing vessel another 4 kg. Table 3 gives a summary of the estimated component masses for a 1 MW engine.

Table 3. Startup System Component Mass Estimates

Component	Mass
Combustion Chamber	15 kg
Condenser	5 kg
Heat Exchanger	10 kg
Additional Piping and Valves	10 kg
Oxygen Tank	15 kg
SUBTOTAL – NO ELECTROLYSIS	55 kg
Electrolysis Unit	15 – 35 kg
SUBTOTAL – WITH ELECTROLYSIS	70-85 kg

3.1.3 RF Subsystem

Our reactor is RF heated, and efficiency in this subsystem will be crucial. Currently, a (linear) series of tube RF amplifiers takes a digitally synthesized waveform and amplifies it. The output is passed through a 90-degree hybrid splitter, a narrow band device that also provides phase control and isolation from load changes. The splitter is tunable over a limited but sufficient range to accommodate changes in plasma impedance. Reflected power is diverted to a dummy load. The source is able to keep the forward power constant despite loading changes. The matching network transforms the impedance of the plasma and RMF coils, a few tenths of an Ohm, to 50 Ohms and survive high voltages and currents. A critical reactor issue is the efficiency of the RF amplification stage.

We propose adopting a new RF drive system using Class E amplifiers based on solid-state switches. Such Class-E amplifiers have achieved over 90% efficiency. The RF drive architecture is shown in Figure 11. It consists of a series of Class-E RF switching amplifiers that feed RF to the antennas via coaxial cables. One set is driven by a square wave, the other by a square wave that is 90 degrees out of phase. This produces the desired sine/cosine drive for the two antenna pairs required for RMF heating and current drive. The waveforms are measured and feedback from these measurements is used to adjust the phasing of the pulse trains that drive the amplifiers. Feedback can also correct for temperature drift of components in the high power stage. This design has the potential to be much more efficient than the linear design described above. Note that the tank (LC) circuit may be common for each antenna.
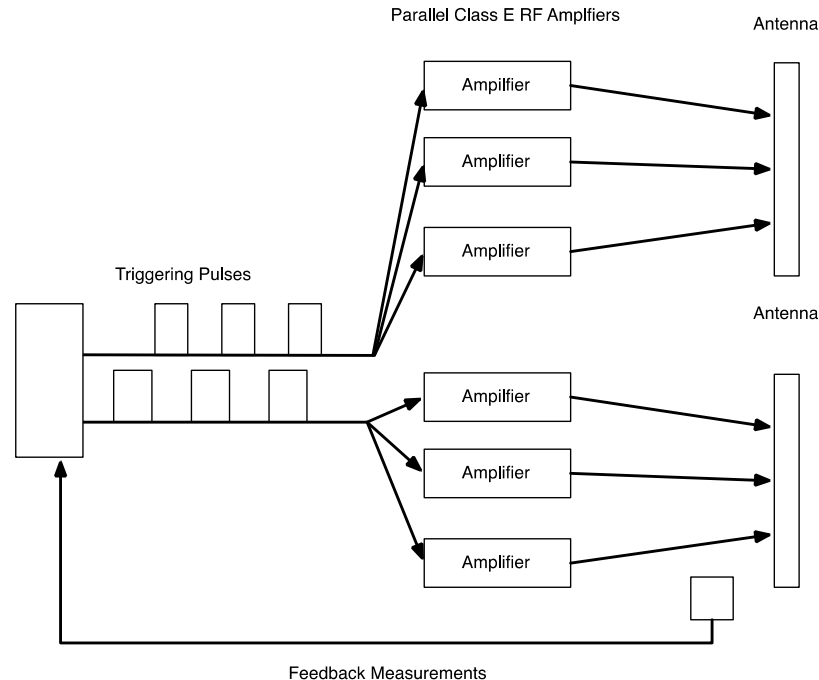
Figure 11. Proposed Class E Amplifier RMF Drive Architecture

Work on sizing the RF system is ongoing. No equipment like this has previously been design for space. Terrestrial systems of 200 kW run about 2000 kg, much of this weight being in cabinets and structures as well as the heavy linear amplifiers. The Class E amplifiers now on the market, which can handle roughly 200 kW, are exceedingly small – 12 x 25 x 40 mm package, literally about the size of a hockey puck. A full RF circuit analysis is required, which we have begun, and hope to continue in our Phase II or potentially a NASA STTR.

3.1.4 Radiators

Current space-qualified radiators will be too heavy but there are upcoming radiator materials that will make the radiators mass a small fraction of the engine total. NASA is currently supporting research in this area, such as the work on carbon-carbon radiators performed by the University of Massachusetts   with the support of the MSFC Center Innovation Fund. (R.W. Hyers 2012) The goal is reduce the areal mass of radiators from about 10 kg/m^2 currently to 2 kg/m^2 or less. Our proposal and Phase I work assumes carbon-carbon radiators with an areal mass of 2.75 kg/m^2 and an average temperature of 625 K.

As a point example, for a 1.1 MW engine assume 400 kW are going to the heat engine and 700 kW out the nozzle, of which 160 kW are going directly to the radiators and 240 kW is useful electric power. Assume the spacecraft has two such engines so the total load on the radiators is 320 kW. Recall that the power emitted by a black body per unit area is proportional to the fourth power of the body temperature T. The total power emitted is then obtained by multiplying by the radiator emissivity and surface area. We assume that both surfaces of the radiator emit so there is an additional factor of 2 in calculating the radiator size.

Equation 1. Black Body Radiation. Power emitted per unit area is equal to the Stefan-Boltzman constant σ times the fourth power of the temperature T. Multiply by the area A and the emissivity ε to calculate the total power Q.

$$Q = A\varepsilon\sigma T^4$$

Assume the radiator emissivity is 1, then the total area required to radiate 320 kW at 625 K is 37 m², or taking into account both the front and back radiator surfaces, a total radiator size of 18.5 m². If there are two wings then each might be 2 m by 4.6 m. With an areal mass of 2.75 kg/m² then both wings together would have a mass of 50.8 kg.

For comparison, consider a traditional system with an emissivity of 0.8, areal mass of 10 kg/m², and a maximum temperature of 400 K. The total area would now be 138 m² and the mass 1378 kg!

Higher radiator temperature means lower cycle efficiency, so cycle efficiency and mass must be traded in the design. Specifically,

3.1.5 Superconducting Coils

Initially, we believed that the mass of the coils would be dominated by the structural mass, and we utilized a virial energy method to estimate the mass. However, when we actually computed the mass of superconducting wire needed using field strength and published properties for wire, we discovered that the wire mass itself could dominate the engine. This raises the question of whether it will be more mass-efficient to use the high-temperature wire that is in the current experimental machine, or use low-temperature wire with the necessary additional cooling. The high temperature wires are superconducting at liquid nitrogen temperatures, around 77 K, while the low temperature conductors require liquid helium cooling to achieve close to 4 K.

This is a subsystem where the space and terrestrial engines may look very different. In the space engine, we will need to taper the coils with the plasma ellipsoid to save mass, while in a terrestrial engine it may save money to have all the coils the same diameter.

Table 4 shows a very simple mass comparison for a HTS and a LTS, just counting turns of the wire at a single radius to produce 3 MA (3e6 A) and parameters from current data sheets. This would produce about a 7 T field at a 0.5 m radius. This does not take into account any packing factor or the reduction in field contribution for the wire that is at a higher radius, but represents an absolute minimum amount of conductor needed. It is important to note that, in most commercial Hi-T superconducting tape, 95% of the mass is in the 5-mil thick stainless steel or copper cladding (on both sides) that encapsulates the 10-µ thick Hi-T material. Companies are now promoting tapes with about ½ the cladding thickness.

Table 4. Superconducting Wire Mass Comparison for a Single 0.5 m Radius Coil

Type	Linear Density	Temperature	Current	Turns	Mass
NbTi 0.7 mm	0.0372 g/cm	4.2 K	350 A	8572	76.7 kg
NbTi 1.04 mm	0.063 g/cm	4.2 K	700 A	4286	84.6 kg
Amperium 12 mm	0.2 g/cm	30 K	700 A	4286	289.5 kg
Amperium 12 mm	0.2 g/cm	77 K	350 A	8572	579 kg

The baseline coil design for the engine has 8 coils distributed evenly over the linear extent of the fusing plasma, on the order of 2 to 8 m. The coil radii follow an elliptical geometry with a maximum radius in the center and minimum at the ends. This is shown in Figure 12.
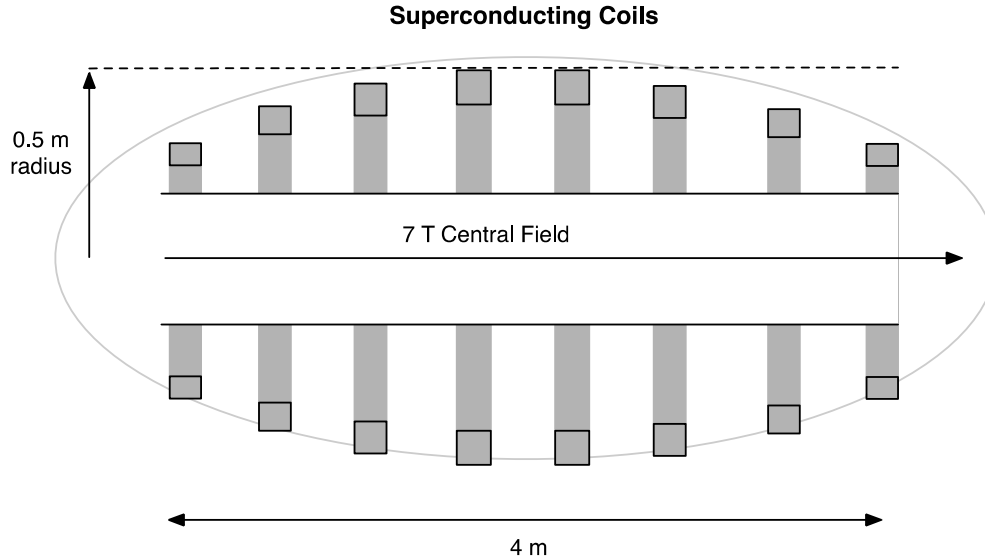
Figure 12 Fusion Solenoid with Ellipsoidal Tapering Coils. The 7 T field strength is at the center of the plasma, r = 0 and z = 0.

We developed an optimization to calculate the currents in coils that minimizes the variation from a mean desired central field. At this point it is not known if the ripple in the field from discrete coils has negative or beneficial effects, or even if the optimal axial field is a constant. In addition, this does not address the radial field variation that we may also want to optimize. However, it is a useful starting point for estimating coil currents. Table 5 gives the currents in each coil for a set of 5 minimum radii, from 0.35 m at a minimum to a maximum of 0.5 m.

Table 5. Coil Currents (MA) for Baseline Coil Geometry with Varying Minimum Radius for a Central Magnetic Field of 7 T

Minimum Radius (m)	0.3	0.35	0.4	0.45	0.5
1	2.66 MA	2.98	3.31	3.64	3.99
2	3.14	3.03	2.94	2.84	2.75
3	2.92	2.93	2.94	2.92	2.91
4	3.01	2.97	2.93	2.88	2.83
5	3.01	2.97	2.93	2.88	2.83
6	2.92	2.93	2.94	2.92	2.91
7	3.14	3.03	2.94	2.84	2.75
8	2.66	2.98	3.31	3.64	3.99

The minimum coil current is seen to be 2.66 MA and the maximum about 4 MA for the different coil radius schemes. If we taper the outer coils enough, the current they require also decreases, but if we maintain the radius of 0.5 m across the length and require the full field strength at the ends then the outer coils would require even more turns than the inner coils. For a final radius of 0.35 m, the current in each coil is nearly constant at 3 MA. If the decreasing radii are taken into

account, then the total conductor mass for 8 coils using 1.04 mm of NbTi carrying 700 A, using the simple turns calculation above, would be 596 kg.

Figure 13 and Figure 14 gives plots for the current optimization algorithm. The B field may not need to be uniform; lower fields may be acceptable at the ends which will moderate the required current in those coils
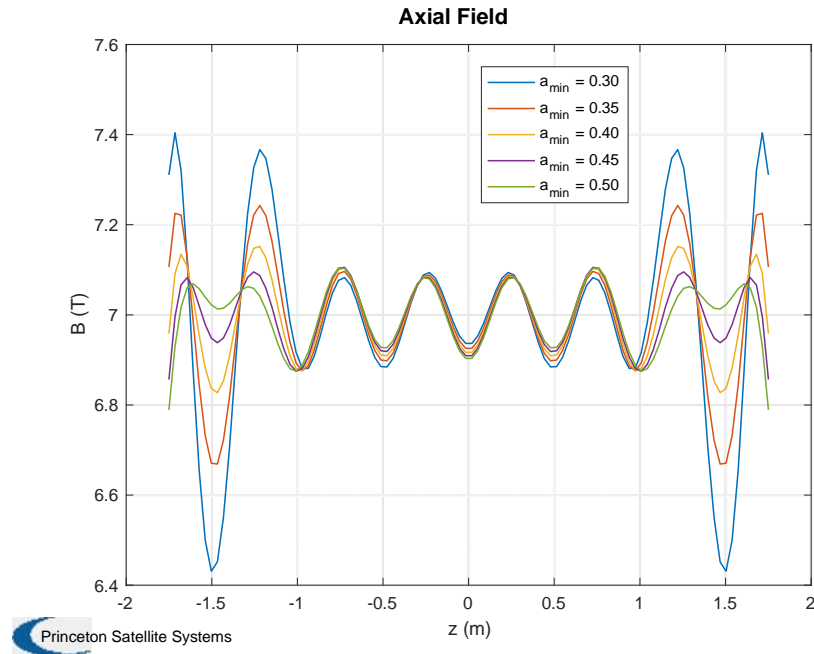
Figure 13. Magnetic Field Shape with Ellipsoidal Solenoid
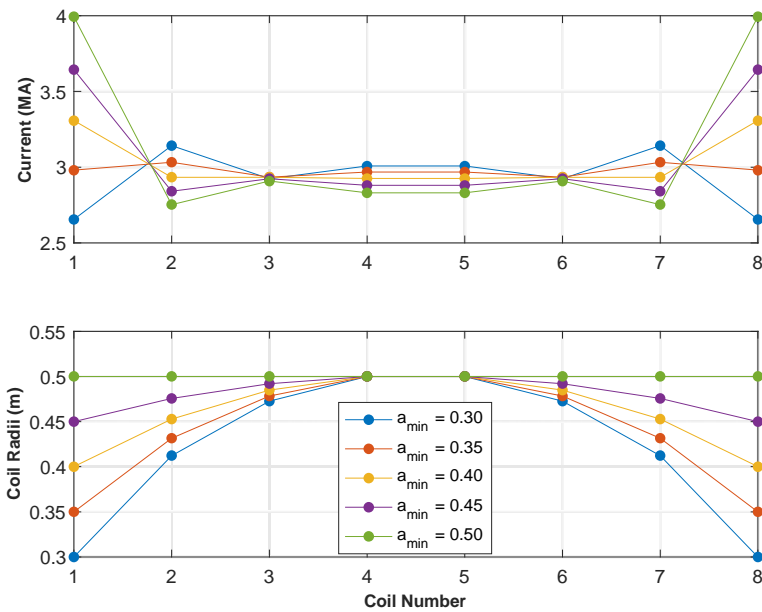
Figure 14. Coil Radii and Currents for Ellipsoidal Solenoid

3.2 Shielding Design

Our prior work on shielding was presented at the 2015 International Astronautical Congress (S. A. Cohen 2015). The neutron flux on the walls of the PFRC is orders of magnitude less than for a tokamak reactor, or other D-^{3}He concepts, but is not zero; for long engine lifetimes or human presence some shielding will still be required.

As neutron absorption cross-sections are many orders of magnitude smaller than their scattering cross-sections, the neutrons must be slowed significantly for attenuation to occur. Findings from Project Prometheus ((Lewis 2006), (A. Bushman 2004) showed that the best materials for neutron attenuation and absorption were low-Z (low atomic number) materials such as hydrogen (possibly in water), lithium, beryllium, and boron, particularly the ^{10}B isotope of boron. Liquid water is an excellent material for neutron shielding, but difficult to handle in low pressure and low temperature environments. For space applications, solid materials are preferable. Solid low-Z material may also serve as liners for the reactor chamber as low-Z elements cause less problematic plasma contamination. These liners must be able to handle the extreme environment of space and also the internal thermal, electrical, and structural conditions in the reactor.

^{10}B strongly attenuates neutron energy and, unlike lithium hydride (LiH) and Be, is also a neutron absorber and therefore reduces the total flux behind the shield. As ^{10}B$_4$C it is a very strong, stable solid over a very large range of temperatures. ^{10}B$_4$C is readily available in nature, safe to manufacture, inexpensive, and it does not exhibit any obvious structural deformities when irradiated. Since it is transparent to x-rays, bremsstrahlung radiation can pass through it to a thermal power conversion system.

X-ray shielding is also required. Many materials absorb X-rays. Tungsten is one of the best attenuators on a per mass basis (Lewis 2006) and meets many of the material requirements for shielding including availability, manufacturability, and high temperature capabilities. The shielding can use thin tungsten sheets.

This initial shielding analysis has focused on limiting the flux at the superconducting coils to a desired lifetime fluence. For ITER, this is 1e22 neutrons/m^2, and for DEMO 3-5e22. The HTS YBCO has an unirradiated critical temperature of about 90 K. In order to maintain this temperature well above liquid nitrogen temperatures of 77 K, a conservative value for the fluence is 6e21 m^{-2}. If the HTS are operated at a much lower temperature, 50 K or 40 K or even less, a much higher fluence can be tolerated. The reduction in critical temperature may be accompanied by a decrease or increase in critical current (M. Eisterer 2009), depending on the operating temperature and local magnetic field strength, making an optimal coil and shielding design a very complex problem.

The required shielding was evaluated using the ATTILA code (S. A. Cohen 2015). ATTILA uses Chebyshev-Legendre quadrature to solve a particle (neutron) transport problem in space, angle, and energy. The model geometry, including material prescriptions, is given to the program and divided into a finite element mesh. ATTILA has a library of energy-dependent neutron cross-sections for over 100 different materials, prepared for the ITER project. The displacements-per-atom reaction rate, activation products, helium production, and heat deposition rates are unique to each material. Meshes were set up for several rocket engine models, one shown in Figure 15.
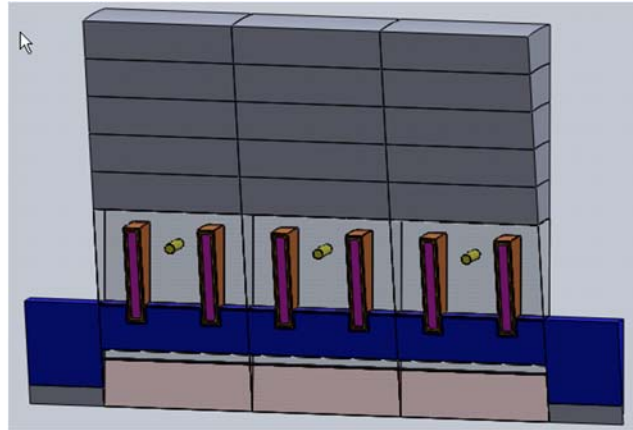
Figure 15. 10 degree segment ellipsoidal FRC reactor model. The plasma ellipsoid has a 25-cm midplane radius. The B4C shielding is cylindrical along the length. The ends of the cylinder are capped with B4C-lined nozzles. Losses out the nozzles are evaluated. Six axial field coils are shown as well as three RMFo antenna segments.

The ATTILA simulations assumed that 1% of the fusion power would be in 2.45 MeV neutrons, a highly conservative value. Our calculations show this number could be reduced another order of magnitude to 0.1%; confirmation of whether the RMF heating method can achieve this requires self-consistent calculations and experimental tests. Hence the amount of shielding is an overestimate. Note that we assumed (enriched) B$_4$C shielding. A further 20% reduction would accrue if pure B were used. The most sensitive element of the rocket structure is the HTS superconducting material. For these, too, we assumed a very conservative value of the tolerable damage (10^{-3} displacements *per* atom, dpa), a factor of 10 lower than assumed by designers of tokamak reactors. This conservative stance was chosen because of the paucity of the available data, which should be remedied in efforts to refine our estimates. For comparison, structural materials, like steel, can tolerate up to 75 dpa. Figure 16 shows results for the DPA versus shield thickness for a 1% neutron power, which is about 3 kW/m^2 for a 1-10 MW PFRC.
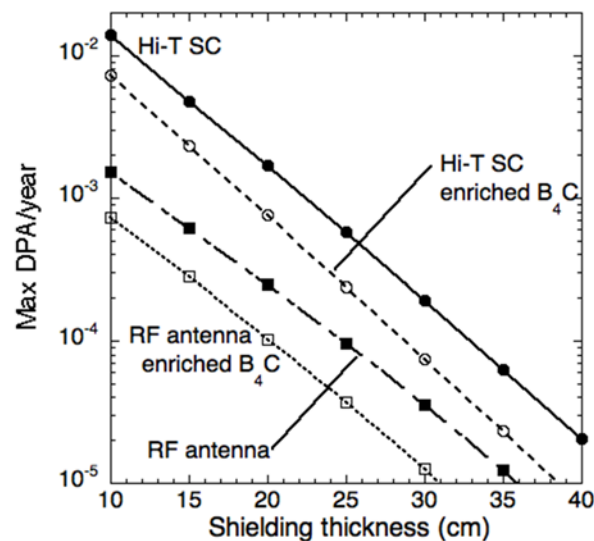
Figure 16. DPA versus shield thickness for the HTS (YBCO) coils and RF antennae.

The ATTILA results indicate that 20 cm of enriched, $^{10}B_4C$ shielding would protect the coils of a 1 MW/m FRC for one year of continuous operation to a dose of 6e21 n/m^2. A 30 year lifespan would require 33 cm of enriched shielding or 39 cm of natural B4C shielding. The tungsten layers required to absorb the bremsstrahlung radiation x-rays, on the order of magnitude of 0.5 to 1 cm thick, reduces the fluence by another 7 to 14%. ATTILA showed the neutron losses through the axial ports to be small, around 0.5% of the total flux. The energy distribution of these neutrons is relatively mild, so the shielding requirements at the end caps is only half that of the center.

If we assume optimistic instead of conservative conditions, we can first extend the lifetime afforded by the shielding ten times if the neutron fluence is ten times less. So if we are able to achieve a 0.1% neutron power through differential RMF heating of the two fusion fuels (deuterium and helium-3), the 20 cm of boron carbide would be sufficient for 10 years of operation. If we run the HTS at a low temperature such that they can absorb an order of magnitude higher fluence, 6e22 /m^2, we can reduce the shielding further, likely by another factor of 2. Therefore, we use about 10 cm of $^{10}B_4C$ shielding in our current engine models.

The thickness of the shielding is a driving factor in the DFD mass, not just because of the shielding mass itself, but because it needs to be internal to the magnetic coils; increasing the radius of the coils increases the currents required to produce the central field, and hence the coil mass.

Table 6 gives masses for the shielding at different thickness. One column gives a simple cylinder while one gives the mass if the shielding is tapered. The plasma radius is 25 cm, so allowing for the scape-off-layer, the shielding starts at a radius of 32 cm. In the case of a tapered shield, the inner diameter tapers to 20 cm at the ends. We approximate this with a stepped cylinder, ½ at the largest diameter and ½ at the smallest diameter. Boron carbide has a density of 2520 g/cm³, lithium hydride 820 kg/m³.

Table 6. Shielding Mass Calculations for a 3 m long FRC

Material	Thickness	Cylinder – ID 32 cm	Stepped – ID 20 to 32 cm
B4C	10 cm	1757.5	1472.5
B4C	20 cm	3990.1	3420.1
Tungsten	0.5 cm	585.1	476.25
Tungsten	1 cm	1179.3	961.56

Further work is required to analyze shielding requirements for additional HTS materials, as well as LTS options, and to examine other materials. Additional irradiation data for the materials to higher fluences is required. The coolant running in channels through the shielding may provide additional attenuation.

3.3 Thrust Augmentation

Student interns at PPPL over the summer and performed 2D simulations using UEDGE, and we were able to utilize this data to produce a functional model of the thrust and specific impulse of

the engine as a function of input power and gas flow rate. Figure 17 shows the latest data. The power levels in the legend are for power into the scrape-off-layer, which is only a portion of the total fusion power.
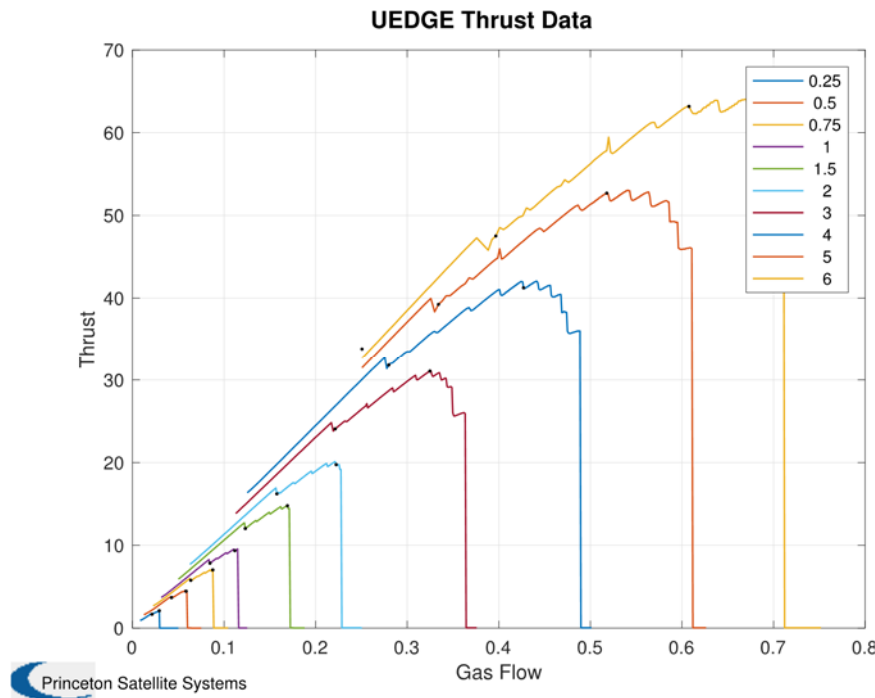
Figure 17. Thrust Data from UEDGE Simulations of SOL Input Power and Gas Flow Rate

The small dots mark the operating range of interest. For each power level there is a fairly narrow range of flow rates which can absorb the power and provide the maximum thrust. We have modeled these regions as linear, with the slope and intercept as a function of input power. This has resulted in the model shown in Figure 18.
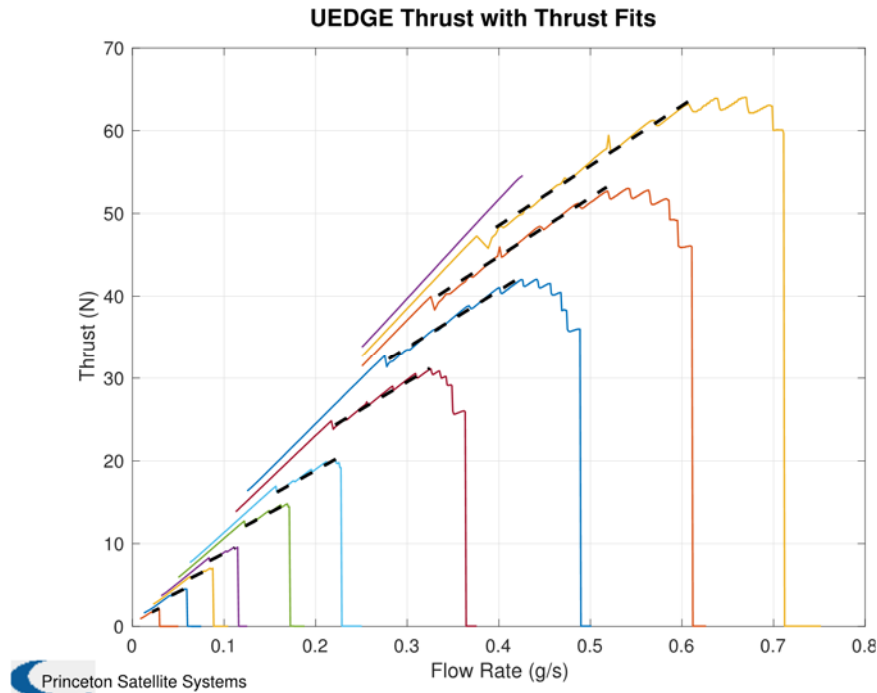
Figure 18. Thrust Model verses UEDGE Simulation Data

Our overall conclusion is that a feasible performance space is 5 to 10 N of thrust per 1 MW of thrust power, with a specific impulse of about 10,000 s. This translates to 2.5 to 5 N of thrust per megawatt of fusion power. Figure 19 shows the thrust model for a 1 MW power input. The specific impulse ranges from 8600 to 9200 seconds.
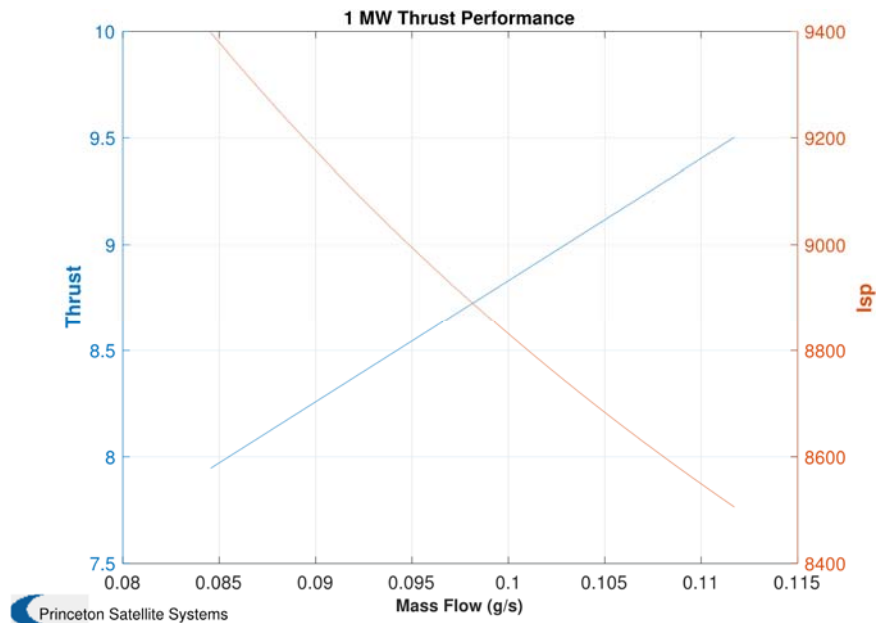
Figure 19. Thrust Performance for a 1 MW Power Input

Figure 20 shows a 4 MW power input. The specific impulse now ranges from 10,000 to 12,000 seconds.
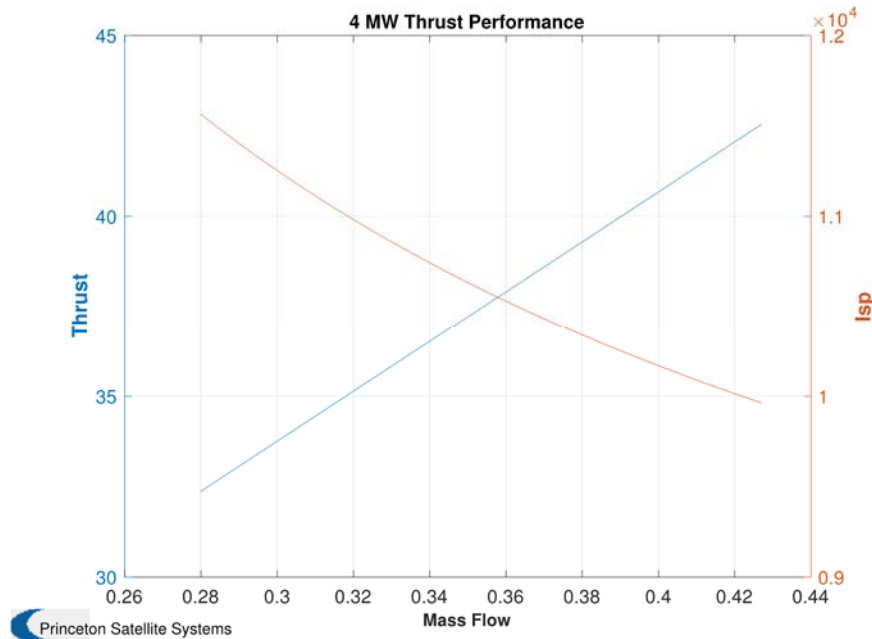
Figure 20. Thrust Performance for a 4 MW Power Input

The efficiency increases both as the flow rate increases, at any given power level, and for higher power levels. Figure 21 shows the efficiency calculated from the model for 1 MW, 2 MW, and 4 MW power levels.
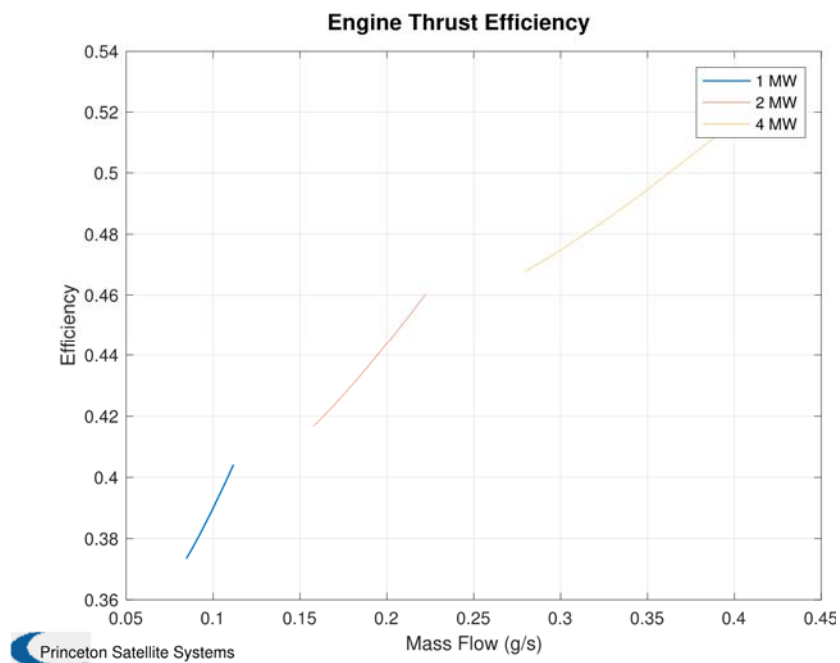
Figure 21. UEDGE Thrust Efficiency from Input Power

Figure 22 shows the velocity model against the UEDGE data, where the bulk exhaust velocity is calculated from the thrust divided by the flow rate. The trend of higher specific impulse for higher power level is clear.
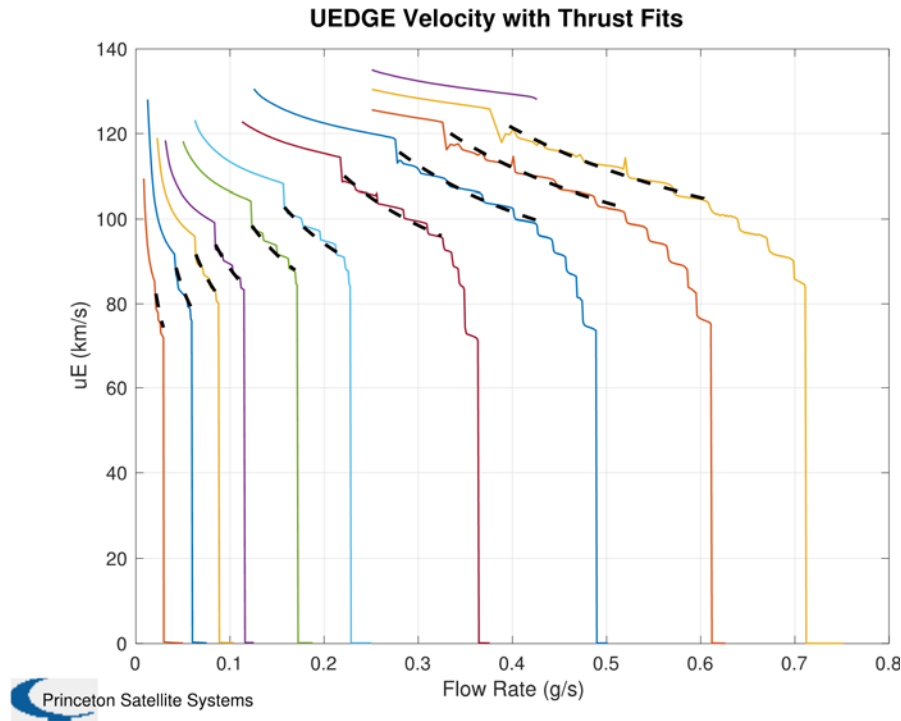
Figure 22. Exhaust Velocity Model Verses UEDGE Data

The model allows us to generate contour plots for expected performance as a function of input power and flow rate. Figure 23 and Figure 24 shows contours for thrust and exhaust velocity, respectively.
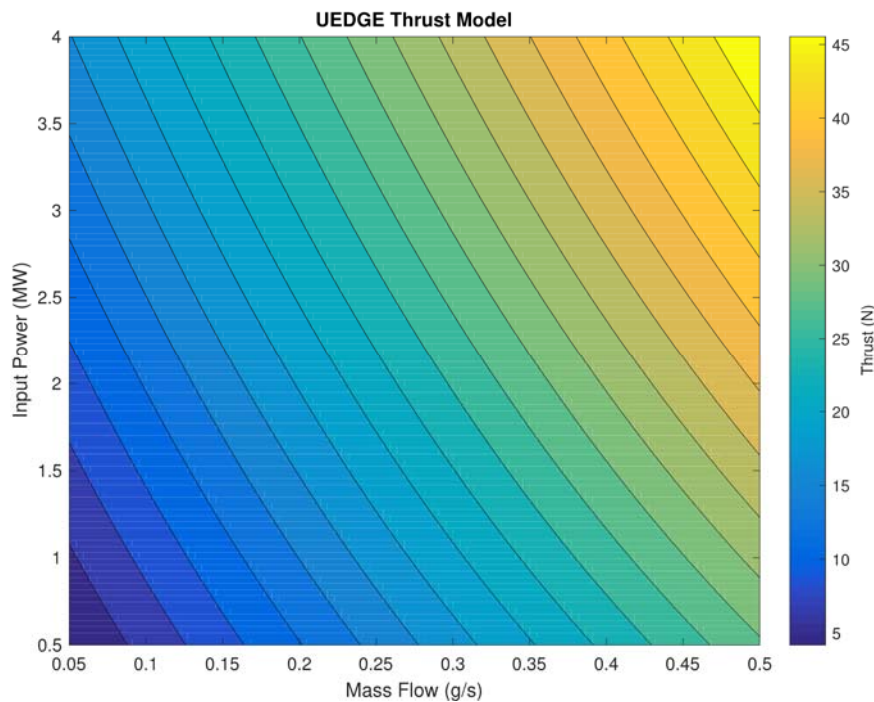
Figure 23. Thrust Contours from UEDGE Thrust Model
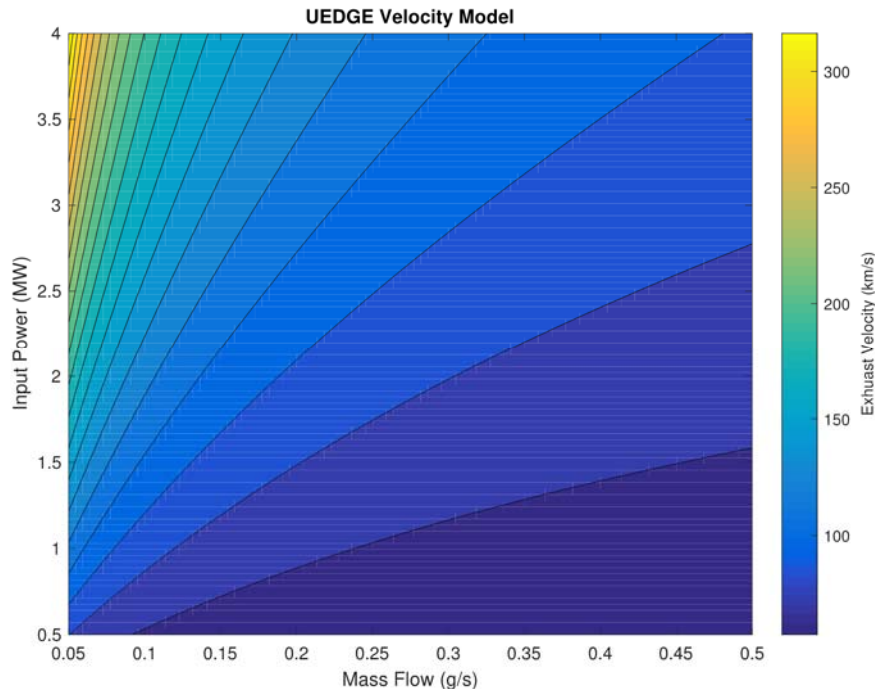
Figure 24. Exhaust Velocity Contours from UEDGE Thrust Model

3.4 Optimal Pluto Trajectory

We used several approaches to further analyze potential trajectories to Pluto and determine if they are feasible with a 1-2 MW engine. Our initial analysis used a Lambert impulsive burn approach; burns on the order of 100 days with thrusts of 50 N could reach Pluto in 4 or 5 years. We next analyzed straight-line trajectories, with a constant thrust and a switch time between acceleration and deceleration phases. We separately studied both Pluto insertion spirals and Earth departure spirals. Finally, we did a simple optimization of a planar trajectory, which takes into account the initial motion of the Earth.

The power relationship for an electric thruster is shown in Equation 2:

Equation 2. Power is equal to one-half the thrust T times the exhaust velocity v, divided by the efficiency N

$$P = \frac{1}{2} \frac{Tv}{N}$$

In the case of DFD, efficiency N is a function of thrust. Therefore the trade between thrust and exhaust velocity is more complex. As an approximation we always start with an assumed constant efficiency in the range of 0.25 to 0.5.

3.4.1 Lambert Impulsive Trajectory

For our NIAC Phase I proposal, we initially calculated an impulsive trajectory to Pluto using Lambert's law. Lambert's law is used for an array of start dates and time of flights, and a minimum delta-V is found. For instance, a 4 year trajectory with a start date in the next 40 years was found to require between 60 and 80 km/s delta-V. We then calculated the mission mass

based on an estimate of specific power, thrust efficiency, and a target payload of 1000 kg. This requires an iteration on the thrust and fuel mass given a burn duration, for instance a 15% burn duration of the 4 year time of flight is 220 days. A delta-V of 70 km/s can be achieved with a thrust of 20 N and a specific impulse of 10,000 s in the allotted 220 days, with a total mission mass of less than 8000 kg, indicating initial feasibility. Table 7 and Table 8 show the complete example mission, with the inputs in the first table and the outputs in the second. The planet positions are calculated for the date given using simple almanac functions.

Table 7. Lambert Analysis Example Mission Inputs

Parameter	Value
Launch Date	March 21, 2036
Payload Mass	1000 kg
Flight Time	4 years
Total Reactor Power	2 MW
Engine Specific Power	0.71 kW/kg
Thrust Efficiency	0.5
Tank Structural Fraction	0.02
Burn Fraction	0.15

Table 8. Lambert Analysis Example Mission Results

Parameter	Value
Lambert Delta-V	65.7 km/s
Burn Duration	219.2 days
Thrust	20.1 N
Specific Impulse	10141.6 s
Engine Mass	2816.9 kg
Fuel Mass	3695.2 kg
Total Mission Mass	7586.0 kg
Deuterium Volume (liquid)	22.6 m^3
Helium 3 Mass	0.4 kg

3.4.2 Straight Line Trajectory

We derived a formulation of a minimum mass optimization for a straight-line trajectory. This is interesting because it finds a value for a constant thrust that will be applied for the entire mission, with a switch in direction at a point somewhat more than halfway to the destination. This is probably a better model for how the fusion engine can operate than two short burns of higher thrust at the beginning and end of the trajectory.

The inputs to the optimization are:
- Straight line distance traveled
- Payload mass (kg)
- Duration (s)
- Exhaust velocity (km/s)
- Fuel structural fraction

- Specific power (W/kg)
- Thrust efficiency

The outputs are the switch time, thrust, and resultant masses for the engine and fuel. A small change in the exhaust velocity results in a big change in the fuel mass required. Figure 25 gives an example result, arriving at Pluto in three years using 4.19 N thrust and 0.4 MW. The payload is seen to be 1000 kg and the total wet mass as 6998 kg. This is for a specific power of 700 W/kg, a thrust efficiency (conversion of output power to thrust) of 0.5 and an exhaust velocity of 100 km/s (specific impulse of 10,000 s). The fuel structural fraction is 0.02.
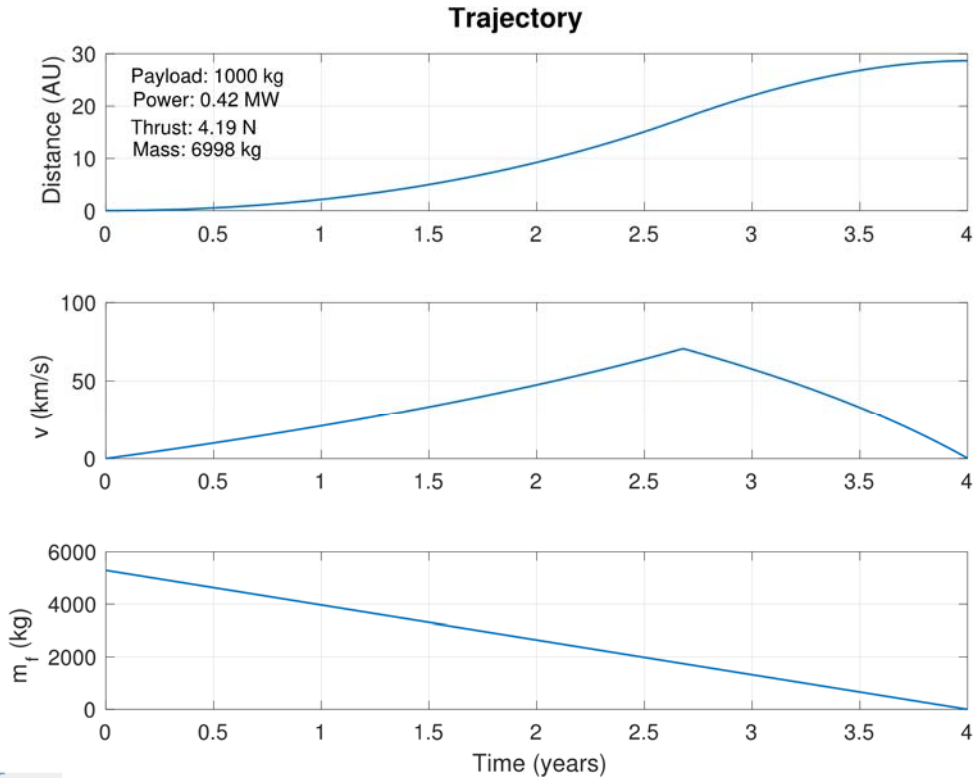
Figure 25. Straight Line Trajectory Example. Specific power is 1000 W/kg, thrust efficiency is 0.3, and exhaust velocity is 100 km/s.

Table 9 and Table 10 provide the numbers for a specific example. In this case the distance traveled is taken to be the distance to Pluto at perihelion, when Pluto is 29.6 AU from the sun, or about 28.6 AU from Earth.

Table 9 Straight Line Example Mission Inputs

Parameter	Value
Distance	28.6 AU
Payload Mass	1000 kg
Flight Time	4 years
Engine Specific Power	0.7 kW/kg
Thrust Efficiency	0.5

Tank Structural Fraction	0.02
Exhaust Velocity	100 km/s

Table 10 Straight Line Example Mission Results

Parameter	Value for Duration of 4 years	Value for Duration of 3.5 years
Delta-V	141.16 km/s	163.5 km/s
Switch Time	2.68 years	2.43 years
Thrust	4.19 N	9.75 N
Power	0.42 MW	0.97 MW
Engine Mass	598 kg	1392.4 kg
Fuel Mass	5287 kg	10765.5 kg
Total Mass	6991 kg	13373.3 kg
Fuel Flow Rate	0.04 g/s	0.1 g/s

The values in Table 9 were chosen to aid in comparison to the Lambert results in Table 7. The flight duration is 4 years and the specific power is 0.7 kW/kg. In fact, the engine is too small, requiring only 0.37 MW, while the minimum size for one engine is likely 1 MW. We would like to have two engines for redundancy. The engine mass decreased while the fuel mass increased. The third column of Table 10 gives the results for a shorter duration of 3.5 years, which returns a more plausible 0.8 MW. Table 11 gives summary results for some more cases with different durations and payload masses.

Table 11. Straight Line Trajectory Results. For these results, the specific power is 1000 W/kg, the exhaust velocity is 100 km/s, and the thrust efficiency is 0.4.

Payload (kg)	Duration (years)	Thrust (N)	Power (MW)	Mass (kg)
2000	4	7.8	0.97	13009
1000	4	3.9	0.49	6504
1000	3.5	8.3	1.04	11391
1500	3.5	12.45	1.56	17086
250	3	18.68	2.33	20623

The plots below show a further exploration of the parameter space from a fixed point solution with a duration of 3.5 years, a payload of 1000 kg, an exhaust velocity of 100 km/s, a specific power of 1000 W/kg, and an efficiency of 0.4. The point solution is marked on each plot with an asterisk. The final plot shows the total mass for each of the studies, which varies between 5,000 and 30,000 kg.
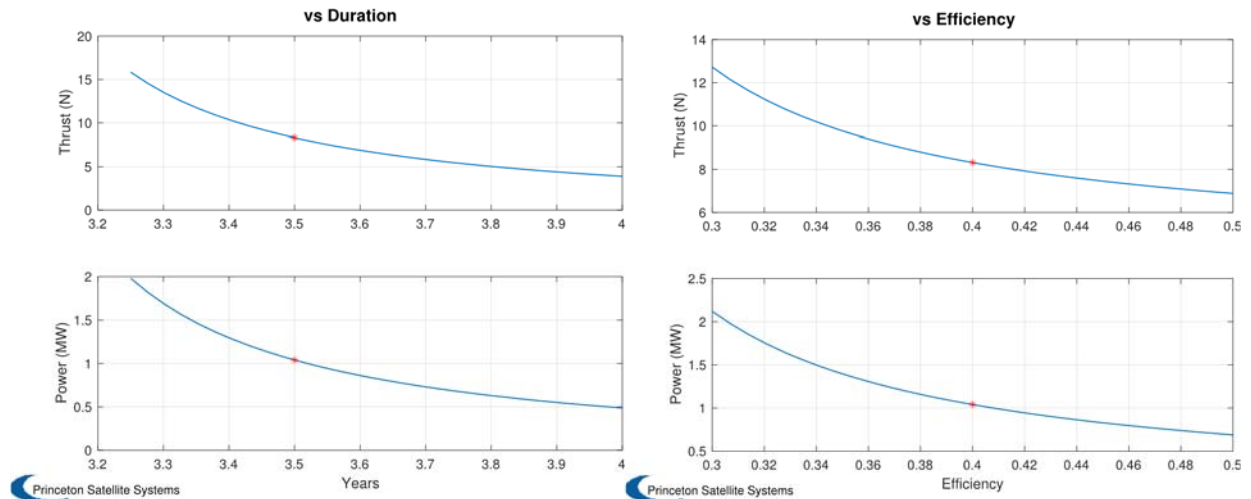
Figure 26. Variation of straight-line thrust and power with flight duration, on the left, and thrust efficiency, on the right.
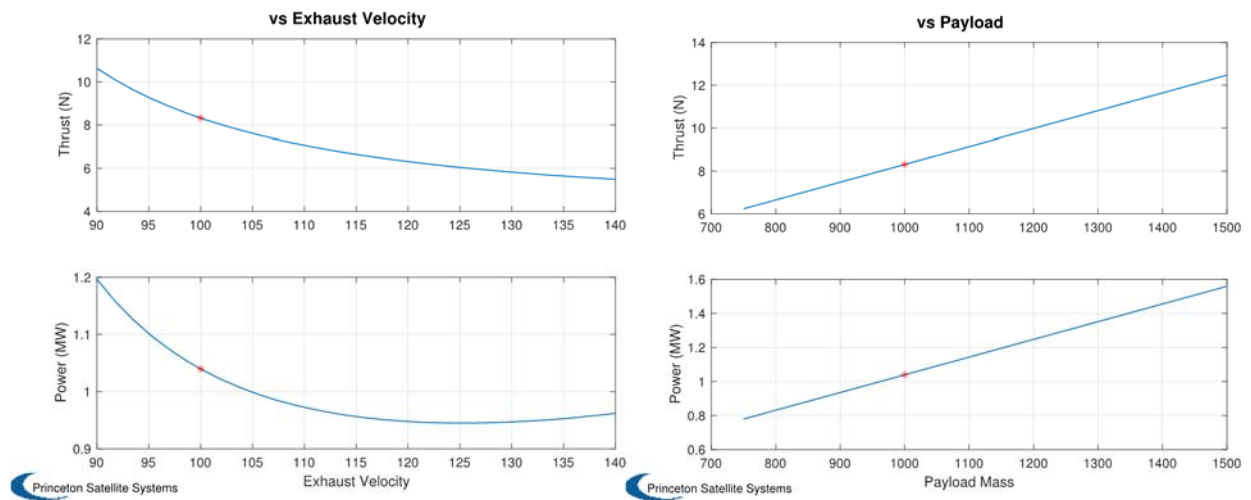
Figure 27. Variation of straight-line thrust and power with exhaust velocity, on the left, and payload mass, on the right.
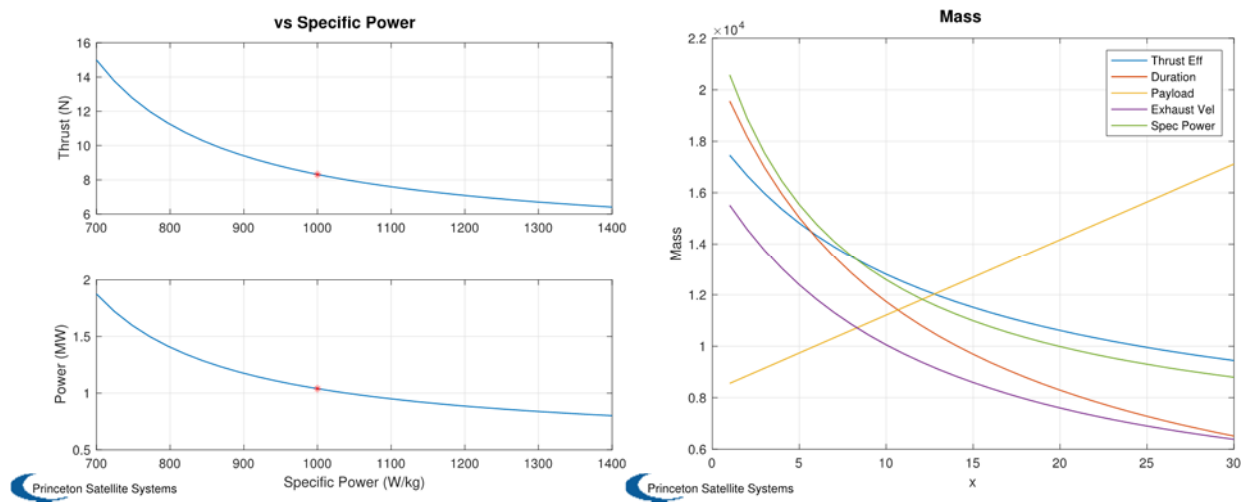
Figure 28. Variation of straight-line thrust and power with engine specific power, on the left, and a comparison of the total mission mass for all study variables, on the right.

We see that increasing the mission duration, thrust efficiency, exhaust velocity, or specific power all reduce the thrust and mass required for the mission. Increasing the payload obviously has the reverse effect.

3.4.3 Pluto Insertion

We wrote a 2D optimization to study the Pluto insertion from a hyperbolic approach with a fixed thrust and mass. The question to answer is, will it be possible to insert into orbit using the relatively low thrust of 5-10 N, and how much time and delta-V should be allocated. Our study has indicated that insertion will require less than 1 km/s delta-V, which is a small portion of the mission total. It is easily accomplished in about one day with 20-40 N thrust and in 2-3 days with 10 N thrust.
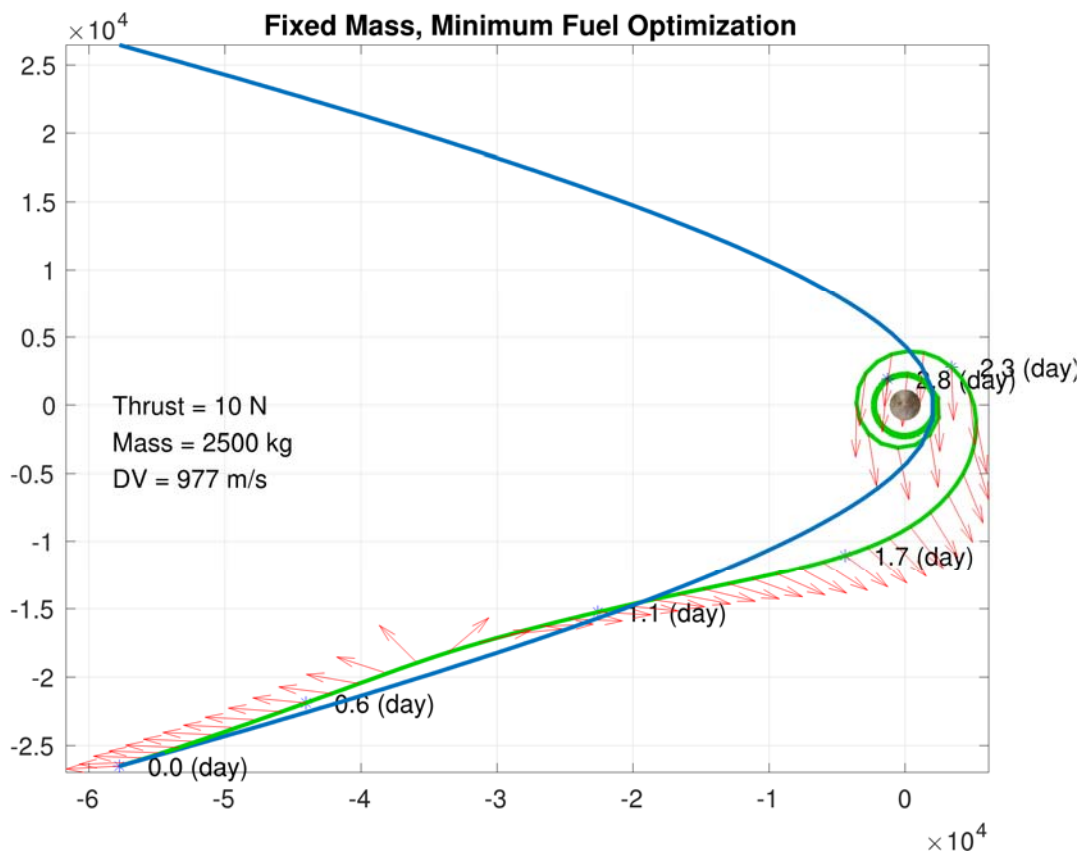
Figure 29. Results for a fixed mass, minimum fuel optimal insertion into Pluto with the following parameters: thrust of 10 N, mass of 2500 kg, resulting in a duration of 2.8 days and delta-V of 977 m/s.

3.4.4 Earth departure

The original concept in our NIAC proposal was to insert the Pluto spacecraft directly into heliocentric orbit. This required a Delta IV Heavy class booster. Analysis shows that an Earth departure from LEO uses very little fuel and takes between 25 and 60 days depending on engine parameters and vehicle mass. This allows a launch by almost any launch vehicle, dramatically reducing launch and overall mission costs. It also allows checkout and testing in low Earth orbit.

A sample departure spiral is shown in Figure 30 for a thrust of 20 N, exhaust velocity of 120 km/s, and initial mass of 6500 kg. The red disk is the inner Van Allen belt. As can be seen, little time is spent there. The total time in the belt for this case is 6.25 days. The outer belt is not a source of radiation damage.
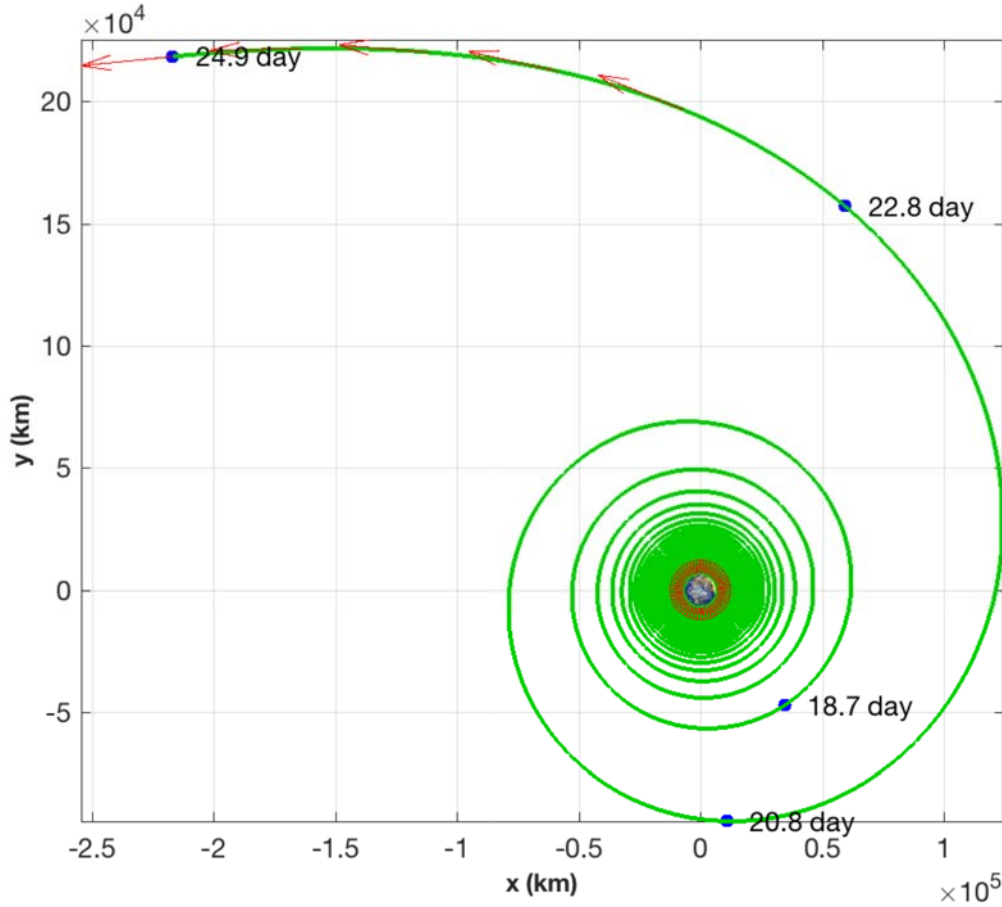
Figure 30. Earth Escape Spiral.
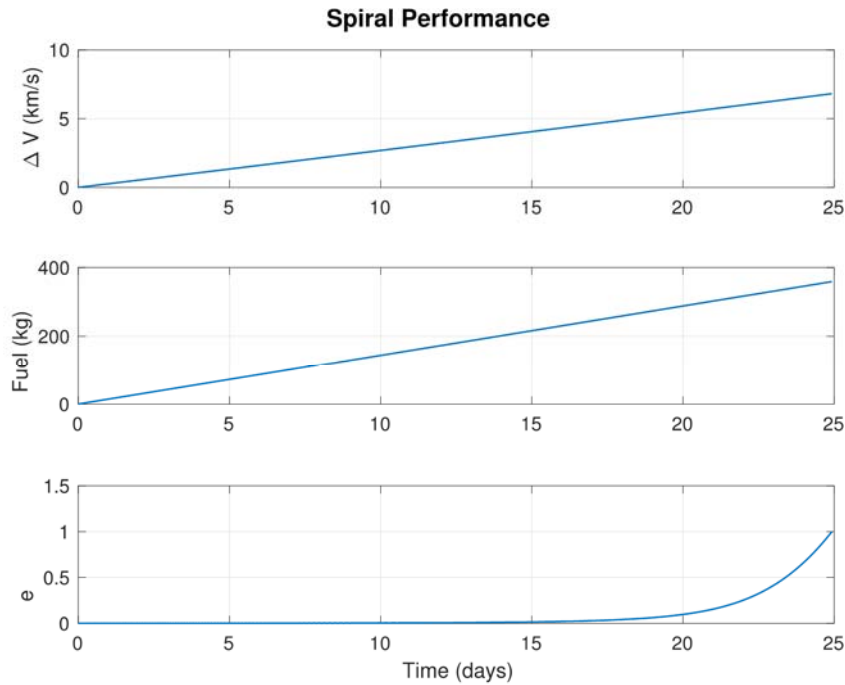
Figure 31 Escape Spiral Delta-V, Mass, and Eccentricity

Table 12 shows results for spirals for several different configurations. The initial altitude is 386 km. The time in the inner radiation belt is calculated as the time between 1000 and 6000 km altitude. The delta-V for the spiral is about 7 km/s in all cases. Note that lower thrust doubles the time of the spiral but only modestly increases the fuel consumption if the exhaust velocity is the same. A lower the exhaust velocity significantly increases the fuel consumed without affecting the time. The model used is a planar point mass orbit with a fixed-step integration. The integration stops when the eccentricity reaches 1.

Table 12. Departure Spiral Results

Initial Mass (kg)	Exhaust Velocity (km/s)	Thrust (N)	Spiral Time (days)	Fuel Used (kg)	Time in Belts (days)
6500	120	20	24.92	358.91	6.25
6500	120	10	50.82	365.89	12.49
6500	100	10	50.51	436.44	12.47
8500	100	10	66.49	574.45	16.30

The DFD solenoid interacts with the Earth's magnetic field and produces a substantial disturbance torque during the Earth spiral. Figure 32 shows the 3-axis torque and its magnitude for a 380 km equatorial parking orbit.
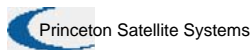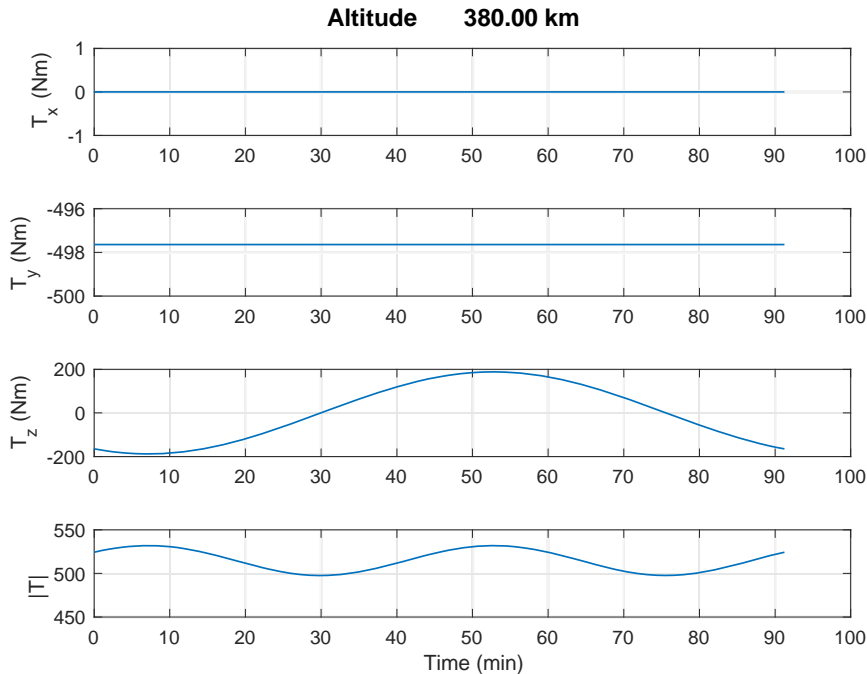
Figure 32. Dipole torque due to the Earth's magnetic field.

The fields produced by the engine do result in a substantial disturbance torque while the engine is in Earth orbit. This has to be compensated for the departure spiral to work. The engine is assumed here to have eight coils each with a radius of 0.5 m and current of 3.2 MA. The magnitude is between 500 and 550 Nm, but the torque is not along the axis of the engine (x in the plot), but perpendicular to it. There are several possibilities for dealing with this torque as the vehicle departs the Earth, which we have not yet explored in detail. One, additional coils could be added to produce correcting torques that are only operated in planetary orbit. Two, magnetic shielding could be applied around the engines, possibly using Hyperco-50 which has a high relative permeability. Three, reaction wheels or control moment gyros could handle the periodic components of the torque. Four, magnetic steering of the plume could provide a small amount of correcting torque. Five, the vehicle could have a reaction control system.

This clearly indicates that it is important to use the absolute minimum magnetic field strength possible when designing the DFD. If the field can be tapered at the ends of the machine, it should be. This will also apply to operations about other planets with magnetic fields, such as Jupiter.

3.4.5 Planar Optimal Trajectories

We wrote a direct method optimization to reach a planar target in a fixed amount of time, with constant thrust and minimum mass. The mass is the combination of the fuel mass, engine mass, payload mass, and accounts for a fuel tankage fraction. The inputs are the specific power, initial and final radii, exhaust velocity, and thrust efficiency. There are a fixed number of points along the trajectory, and the degrees of freedom are the thrust angle at those discrete points. In MATLAB, this is solved using the *fmincon* function in the Optimization Toolbox. Figure 33

shows an example trajectory generated this way, which shows that the orbit follows a good
portion of the Earth's orbit before it peels away in the direction of Pluto. From thereafter, it
resembles the straight-line trajectory.
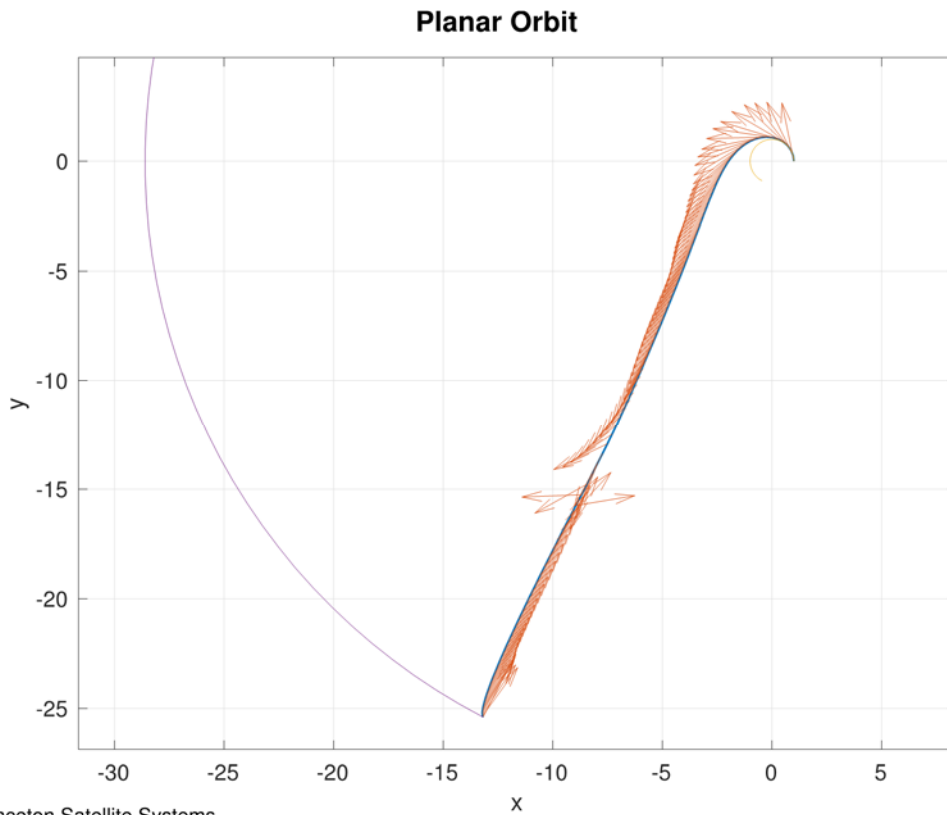
Figure 33. Planar trajectory with thrust arrows. The change in direction of the thrust at the switch
time is easily seen. The trajectory follows Earth's orbit for some time before following a nearly straight
trajectory to Pluto.

Figure 34 shows the time history plots of the radial velocity u, tangential velocity v, radius r (in
astronomical units), fuel mass m_f, and thrust angle φ. The radial velocity plot is very similar to
the straight-line trajectory results, which is to be expected. The tangential velocity initially
increases, and then begins decreasing after about 0.3 years. This example uses the same
parameters are our previous solutions: 1000 kg payload, 4 year duration, exhaust velocity of 100
km/s, specific power of 1000 W/kg,

Princeton Satellite Systems
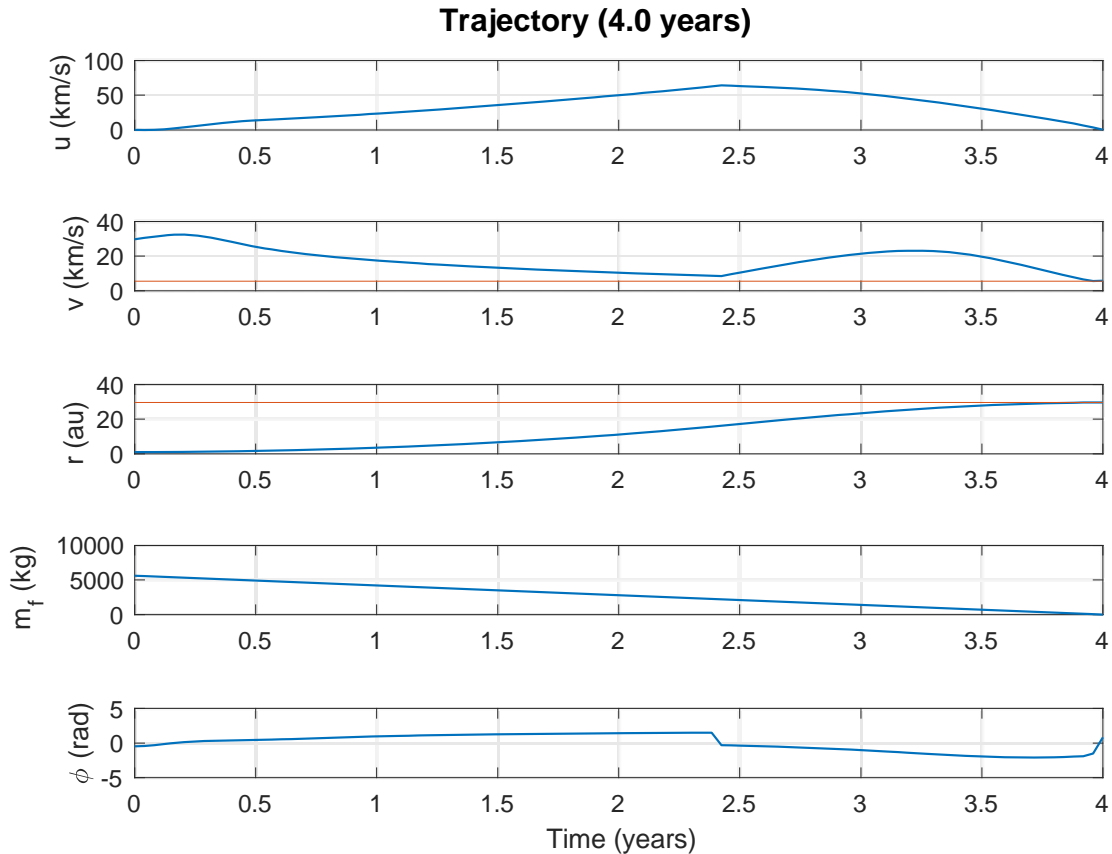
Figure 34. Planar transfer trajectory time histories

Table 13 and Table 14 show parameters for an example planar mission. The solution is close to the straight-line solution, requiring somewhat more fuel.

Table 13 Planar Optimization Example Mission Inputs

Parameter	Value
Distance	29.6 AU
Payload Mass	1000 kg
Flight Time	4 years
Engine Specific Power	0.7 kW/kg
Thrust Efficiency	0.5
Tank Structural Fraction	0.02
Exhaust Velocity	100 km/s

Table 14 Planar Line Example Mission Results

Parameter	Value for Duration of 4 years
Delta-V	143.81 km/s
Thrust	4.45 N

Power	0.44 MW
Engine Mass	635.5 kg
Fuel Mass	5615 kg
Total Mass	7363 kg
Fuel Flow Rate	0.04 g/s

Note that in this case, the thrust is 4.45 N and the engine power is only 0.44 MW. A DFD engine cannot actually be made this small. The next logical step in trajectory analysis is to use a more advanced tool such as NASA's MALTA with the engine model developed in Task 3.

3.5 Updated System Design

We begin this section by discussing our engine design model and presenting updated point designs for both a 1 MW and 10 MW reactor. Then, we present updated vehicle design including mass tables for the orbiter and the lander.

3.5.1 Engine Modeling
We have a MATLAB model of the PFRC reactor that is based on the density and temperature of the fusion reactants and the engine size, so that the engine can be scaled. The inputs to the engine design function are:
- Length and radius of the fusing plasma ellipsoid
- Device beta – ratio of plasma pressure to magnetic pressure
- Number density and temperature of Helium-3
- Number density and temperature of Deuterium
- Electron temperature
- Factors f-D and f-T reducing the fraction of D-D and D-T reactions from what would be expected given the nominal temperature
- Specific mass of the RMF heating system
- Efficiency of power conversion by the RMF drive system
- Fraction of RMF heating power that is deposited into the plasma
- Specific mass of the Brayton power generation system
- Power recycling efficiency
- Specific mass of the coil refrigerator
- Fraction of heat power required to be rejected by the refrigerator
- Gas box power fraction
- Heating power fraction
- Shield thickness factor – meters per MW/m^2 of neutron flux
- Structural factor
- Radiator temperature, emissivity, and areal mass density

The model takes the following steps:
1. Calculate the magnetic field using the plasma parameters (temperature, number density) and beta
2. Calculate the plasma volume and internal wall area

3. Compute the synchrotron radiation power using Bingren's model (Bingren 2005) or the NRL Formulary model with a 10% volume factor
4. Compute the volumetric fusion power, neutron power, and Bremsstrahlung power using a model of the D-Helium-3 reaction, where f-D and f-T reduce the D-D and D-T side reactions for non-homogeneous plasmas
5. Compute the total fusion power, neutron power, and Bremsstrahlung power by multiplying by the plasma volume
6. Compute the gas box power from the total fusion power using the given fractional coefficient; this is the portion of the fusion products power that does not go out the nozzle, but is deposited as heat.
7. Compute the thrust power as the power remaining after the losses due to Bremsstrahlung, synchrotron, neutrons and gas box
8. Compute the RMF input power as a fraction of the total fusion power
   a. Compute the net RMF power deposited in the plasma using the RMF drive efficiency and fractional heating coefficient
9. Compute the total electric power from the loss powers using the recycling efficiency
10. Compute the net electric power as the electric power minus the RMF power
11. Calculate the shielding thickness and mass using the neutron wall loading and the shielding thickness factor
12. Size the magnets using the previously calculated field strength and the inner radius that accounts for the scrape off layer and shielding; this requires an assumption of the wire current and wire linear density.
13. Size the coil refrigeration system from the total power lost as heat using the refrigeration heat fraction and specific mass
14. Size the power generation system using the specific mass and the total electric power
15. Size the RMF heating system using the specific mass and the RMF input power
16. Size the radiators using the heat loss and radiator temperature, emissivity, and areal mass
17. Calculate the additional structure using the structural factor and the sum of the masses of the radiators, magnets, shielding, coil refrigerator, power generation system, and RMF system
18. Calculate a total engine specific power
19. Calculate a total wall loading from the heat

Nominal parameters for our D-Helium-3 engine are given in Table 15, Table 16, and Table 17.

Table 15. Nominal engine plasma parameters

Parameter	Value
Beta	0.88
Scrape off layer thickness	0.05 m
Plasma radius	0.3 m
Plasma length	3.5 m
Deuterium number density	1.4e+20
Deuterium temperature	100 keV
Helium-3 number density	2.8e+20
Helium-3 temperature	100 keV
Electron temperature	30 keV

f-T, factor for Tritium side reactions	0
f-D, factor for Deuterium side reactions	1

Table 16. Nominal engine power parameters

Parameter	Value
Gas box power fraction	0.1
RMF heating power fraction	0.11
RMF drive efficiency	0.9
RMF plasma heating factor	0.5
Synchrotron wall reflection	0

Table 17. Nominal engine subsystem parameters

Parameter	Value
Specific mass of the RMF heating	0.001
Specific mass of the power generation	0.0007
Specific mass of the refrigeration	1e-4
Efficiency of the power conversion	0.6
Shielding thickness factor	50 m/(MW/m^2)
Structural factor	0.1
Radiator areal mass	2.1 kg/m^2
Radiator temperature	625 K
Radiator emissivity	1

The engine design script makes two graphics: a pie chart of the masses and a flow chart of the powers. These are shown in Figure 35 for a 1 MW engine and in Figure 37 for a 10 MW engine. You can see that the power to the "gas box" is exactly 10% of the fusion power, as this is an input parameter.

Figure 35. Engine Mass Pie Chart for a 1 MW Engine.
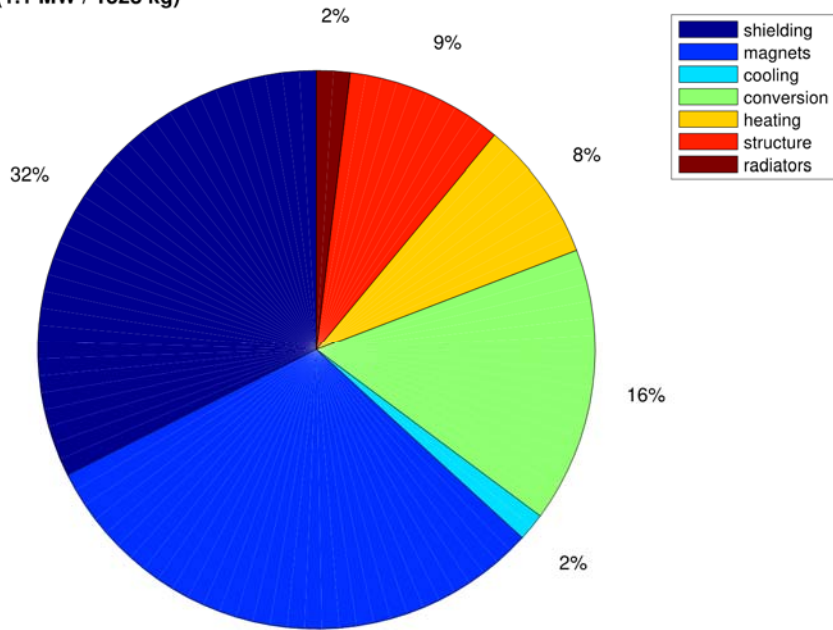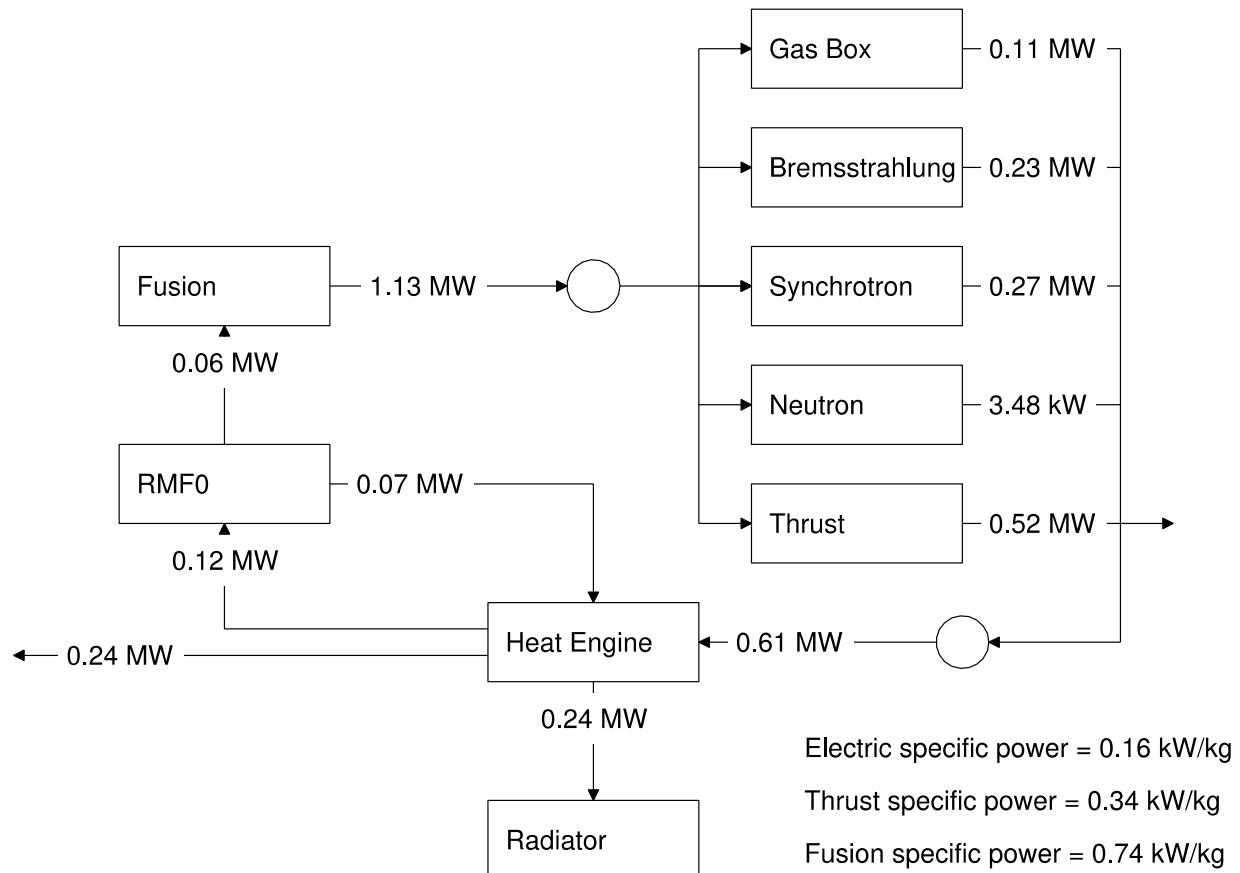

Figure 36. Power Flow Diagram for a 1 MW Engine
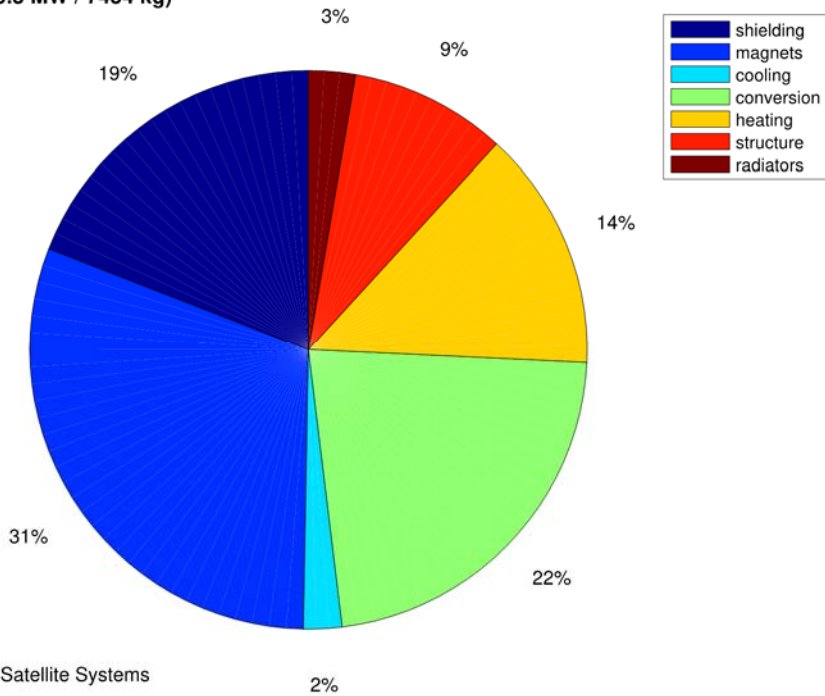
Figure 37. Engine Mass Pie Chart for 10 MW Engine.
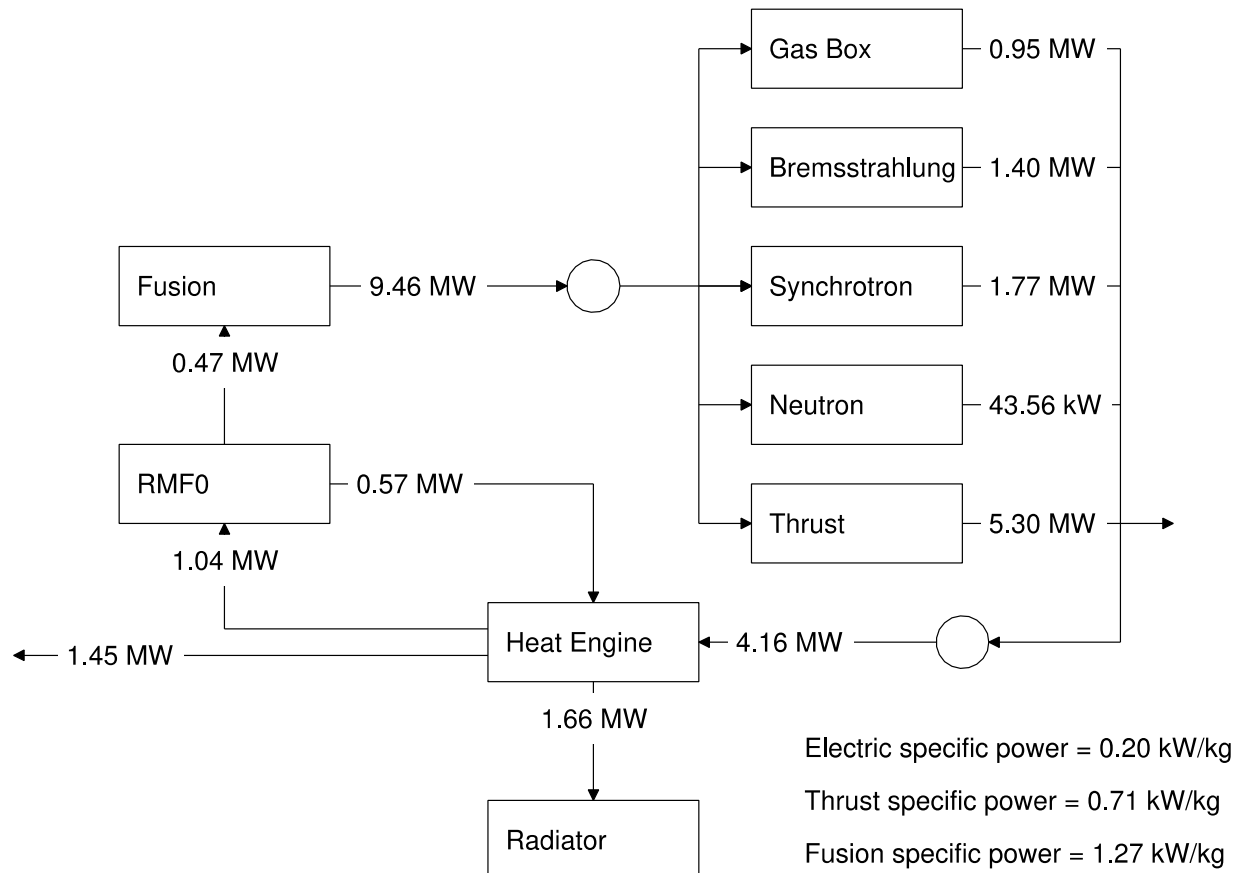
Figure 38. Power Flow Diagram for a 10 MW Engine

The model enables us to look at aggressive verses conservative cases for tritium side reactions, neutron wall loading, shielding, and other subsystems, based on the plasma parameters. We commonly assume that all of the tritium is exhausted before fusing, which is the goal of our engine design, by setting the f-T factor to 0. Changing the deuterium reaction factor f-D from 1 to 0.25, which is a best-case scenario for non-thermal ion distributions from the RMF heating, reduces the shielding thickness, also by a factor of 4. Listing 1 gives an example output.

Listing 1. 1 MW Engine Design Report

```
Plasma Length: 0.8 m
Plasma radius: 0.20 m
Deuterium temperature: 100.0 keV
Helium 3 temperature:  100.0 keV
Electron temperature:  30.0 keV
Deuterium density: 1.05e+20 /m3
Helium 3 density:  3.15e+20 /m3
Electron density:  7.35e+20 /m3
Machine beta: 0.88
Magnetic field: 5.4 T

Total Engine Mass: 1528.09 kg
Total Fusion Power: 1.13 MW
Thrust Specific Power: 0.339518 kW/kg
Engine Specific Power: 0.498120 kW/kg
Fusion Specific Power: 0.739414 kW/kg
Subsystem Masses:
      Shielding Thickness:     10.27 cm
      Shielding:              495.30 kg
      Magnets:                471.04 kg
      Coil Cooling:            24.44 kg
      RMF System:             124.29 kg
      Power Generation:       244.43 kg
      Radiators:               29.67 kg
      Overall Structure:      138.92 kg

Total Fusion Power: 1.13 MW
      0.11 MW Gas Box
      3.48 kW Neutrons
      2.57 kW/m2 Neutron wall load
      0.27 MW Synchrotron Radiation
      0.23 MW Bremsstrahlung Radiation
      0.52 MW Thrust Input Power
Total Thermal Power: 0.61 MW
      Conversion efficiency: 0.60
      Bus Power: 0.24 MW
      RMF Power: 0.12 MW
      Radiated Power: 0.24 MW
```

3.5.2 Engine Layout

We spent some time considering the engine layout, and in particular the relationship between the shielding and the cooling channels for the Brayton engine. Our initial concept was to have the coiling channels run lengthwise along the engine, but we determined that wrapping the coils around the engine makes more sense. This could allow the engine to be constructed in discrete

sections and makes the design more scalable between the minimum (1 MW) and maximum (10 MW) power levels.

Figure 39. Cross-Section of a Coil showing copper sheathing (for current transients) and structural shell
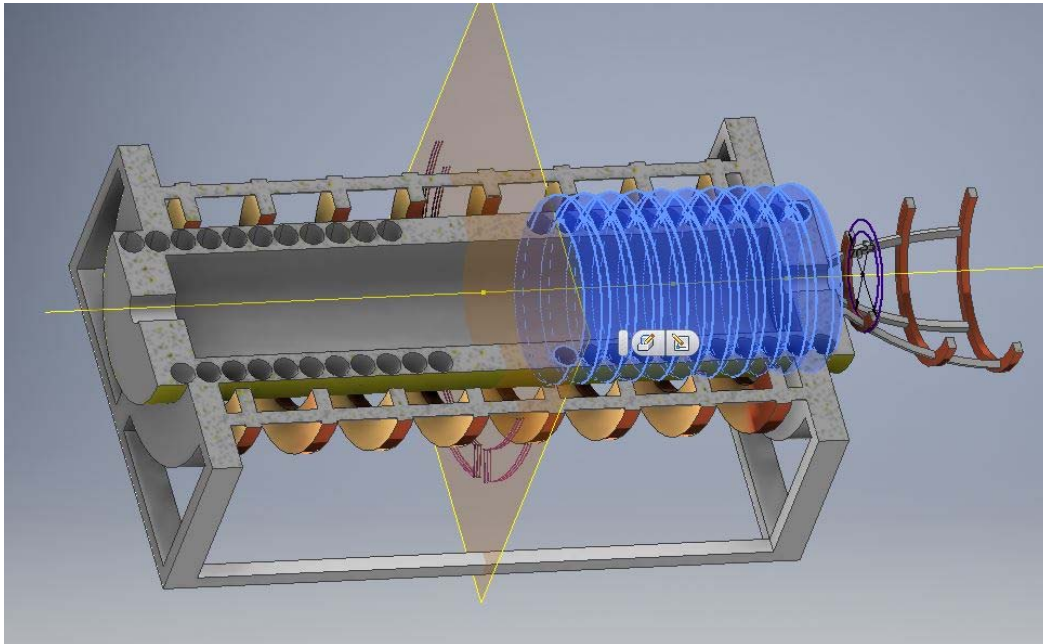
Figure 40. Cutaway view of the engine model showing cooling channels embedded in shielding.
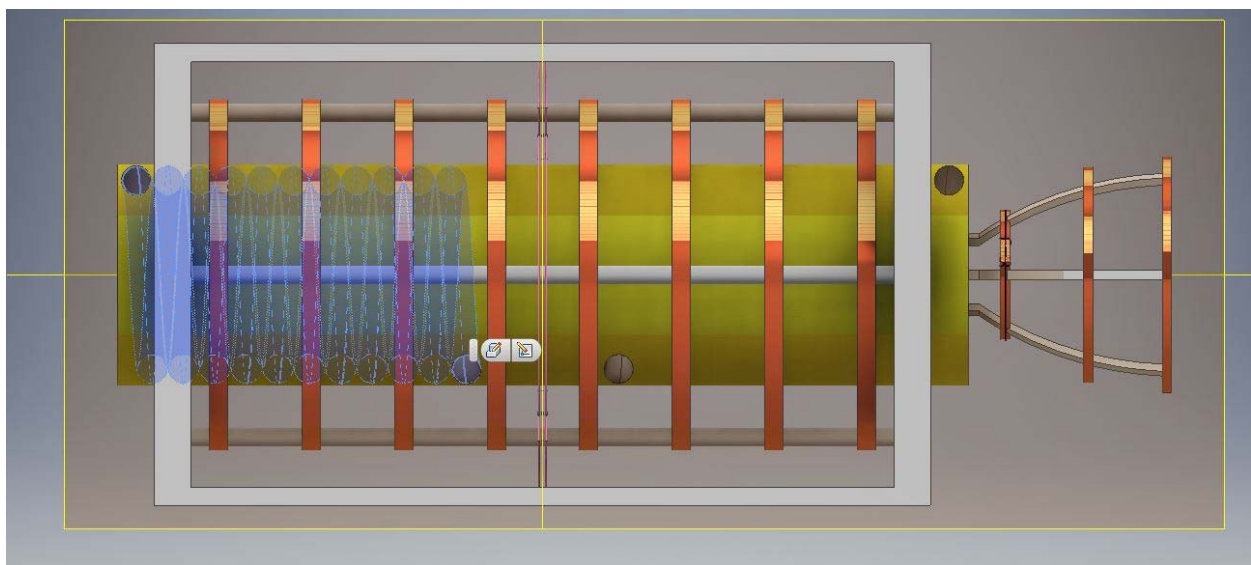
Figure 41. Side View of the Engine Model

Recently, PPPL allocated artist time to produce an updated model of the reactor, both terrestrial and space versions. Figure 42 shows the space rendering with subsystems labeled. The nozzle shaping coils on the left-hand side are notional, they may be much smaller or not needed at all.
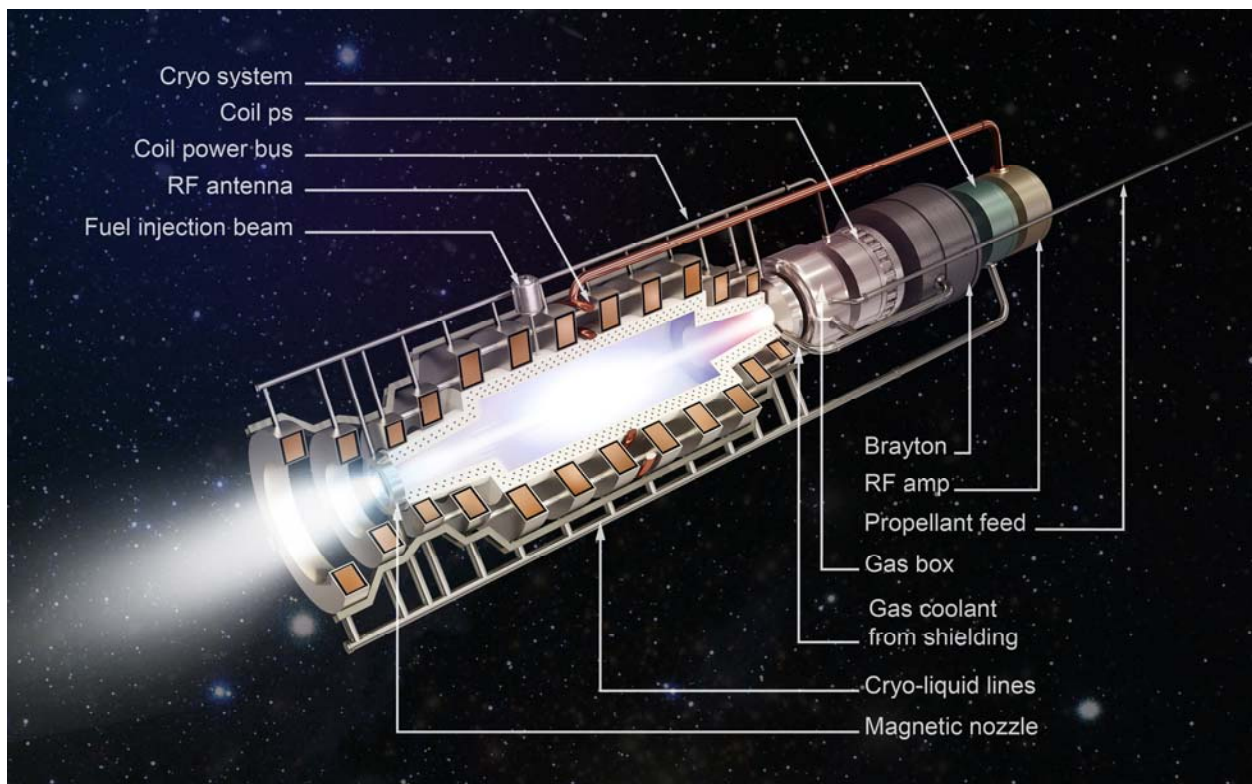
Figure 42. Artistic rendering of the engine

3.5.3 Vehicle Design

The vehicle nominally has two engines at one of the craft with the main bus and lander attached to the other. Figure 43 shows a 3D model generated in MATLAB. The components are grouped

into subsystems for mass properties calculations. The large wings are space radiators, not solar panels. Small solar panels are shown, which are utilized during initial Earth orbit checkout. The large cylinder in the center houses the cryogenic deuterium tank and Helium-3 tank. The Helium-3 tank is shown sized for gaseous storage at standard temperature and pressure. The optical communications lasers are mounted on booms perpendicular to the radiators. In this case the vehicle was sized for two 1 MW engines.
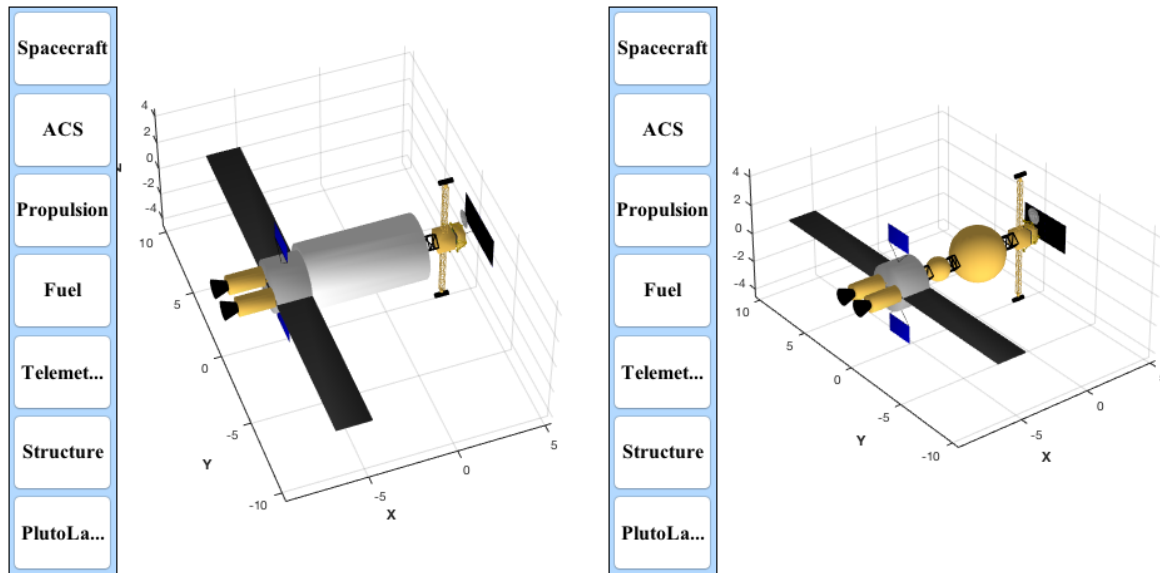
Figure 43. Vehicle CAD Model. On the right, the vehicle without its solar shield, so that the fuel tanks may be seen.

The following design changes were made from our proposal model:
- The engines were made longer to better approximate their true size
- Solar arrays were added for the checkout phase directly after launch
- The optical communications trusses were moved to the bus side of the vehicle
- A factor of 2 was corrected in the radiator sizing, making them longer
- A stowed option was created for the lander solar panels

The radiators were sized using an assumed temperature of 625 K, an areal mass of 2.75 kg/m^2, and an overall power plant efficiency of 0.58. The total heat rejection required is then 840 kW, or 210 kW per side of each radiator wing. This results in a total radiator area of 50 m^2.

Table 18 Orbiter Mass Budget

Component	Quantity	Mass (kg)
Engine	2	1357
Radiators	2	66.75
Magnetic Nozzles	2	71.43
D2 Tank (full)	1	3432
He3 Tank	1	0.22
Insulating Shell	1	200
Optical Truss	2	10

Gimbals	2	3.75
Laser Communication Unit	2	2
Orbiter Payload	1	270
Lander	1	230
TOTAL		**7154**

The goal is for the Pluto vehicle to fit on a single launch vehicle. Published launch vehicle performances are given in the table below.

Table 19. Launch Vehicle Performance

Family	Vehicle	LEO (kg)	ISS (kg)	Escape
Atlas	401	9800	8910	N/A
Atlas	411	12030	10670	N/A
Atlas	421	13600	12060	N/A
Atlas	431	15260	13250	N/A
Atlas	501	8210	7540	N/A
Atlas	511	11000	10160	N/A
Atlas	521	13500	12510	N/A
Atlas	531	15530	14480	N/A
Atlas	541	17410	16290	N/A
Atlas	551	18850	17720	N/A
Delta IV	Medium	9190	851	N/A
Delta IV	Medium+ (4.2)	12900	12000	N/A
Delta IV	Medium+ (5.2)	11060	10220	N/A
Delta IV	Medium+ (5.4)	13730	12820	N/A
Delta IV	Heavy	28370	25980	8000 (MTO)
Falcon 9	Block 1	9000	8500	N/A
Falcon 9	1.1	13150	12420	N/A

3.5.4 Lander Design

The lander is depicted with the solar array deployed on the right of Figure 43. Figure 44 shows just the lander, where the solar panels can be seen to be attached to a long slender truss, which gives them room to rotate for tracking the orbiter during overflights. A 1080 nm laser onboard the orbiter would allow 30 to 50 kW to be delivered to a receiving area of 4 square meters. A single 400 N green propellant engine is used for landing. We estimate the lander might be 200 to 250 kg.
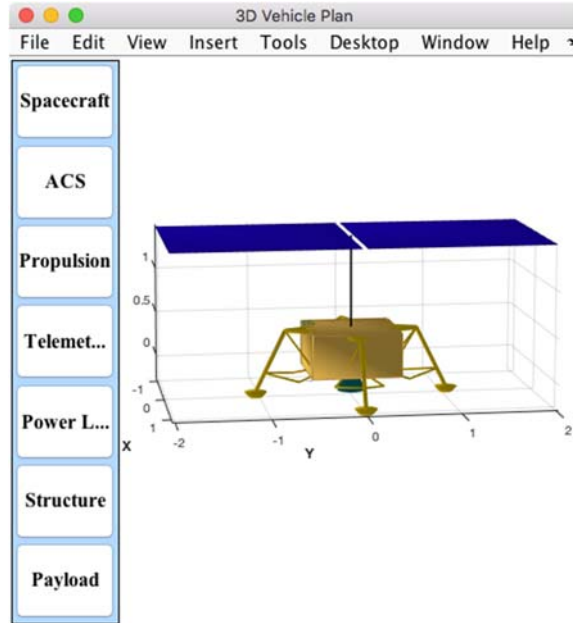
Figure 44. Lander CAD Model. The solar panel is on a truss with a gimbal so that it can track the orbiter during overflights.

Figure 45 shows an analysis of the power beamed to the lander each orbit.
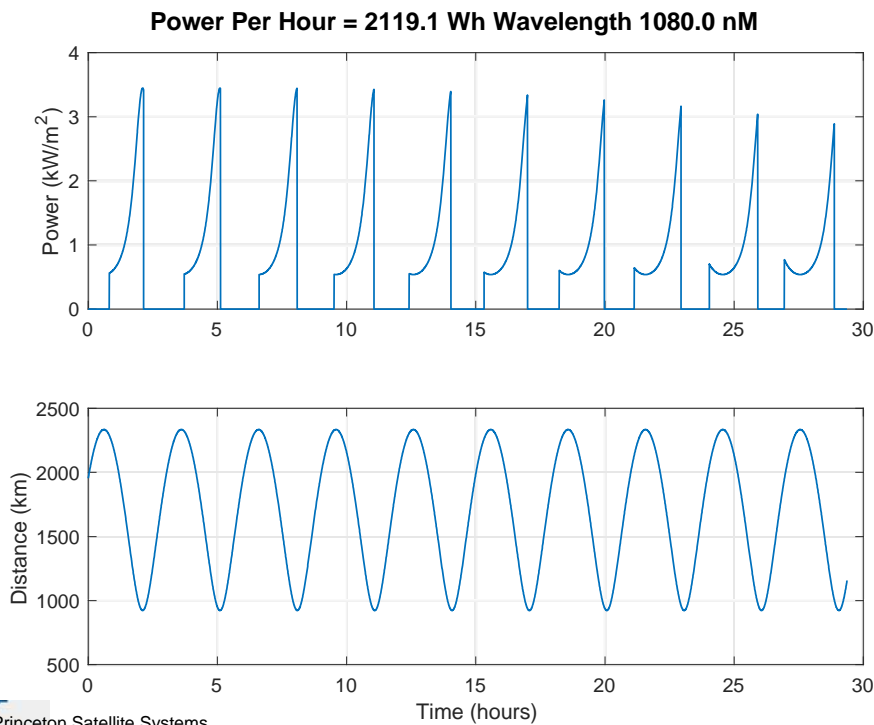
Figure 45. Lander Power Analysis. The power transmitted to the lander is periodic with the orbit.

The scientific instrumentation created for this mission may look quite different from prior missions due to the very large amounts of power that would be available. The instruments would still be mass constrained but having tens or hundreds of kW is unprecedented. We talked to Prof.

Binzel of MIT's Planetary Sciences department about potential instruments for the mission, resulting in the following initial suite: for the orbiter, a combination of the New Horizons instrument suite (imagers, spectrometers, passive radiometer, dust counter) and Rosetta Orbiter instruments, with the addition of a magnetometer and thermal radiometer for measuring surface temperatures and thermal inertias. For the lander, instrument candidates include an instrument like CONSERT from Rosetta, for probing the interior by radio waves, and a drill.

The lander is anticipated to have the following components.
- Solar array on a gimbaled truss
- Battery
- Two omni antennas
- Green propellant thruster (Isp 285 sec)
- 8 to 12 RCS thrusters
- Two green propellant fuel tanks
- Two star cameras
- IMU

We have simulated a landing trajectory using this thruster from a 20 km altitude. The simulation assumes a specific impulse of 285 sec and an acceleration of 2 local g's, resulting in a thrust of 380 N. The landing with a linear tangent law takes about 13 minutes and consumes about 88 kg fuel (200 kg total vehicle mass). The delta-V is about 1 km/s. If two fuel tanks are used each would have a radius of about 20 cm.
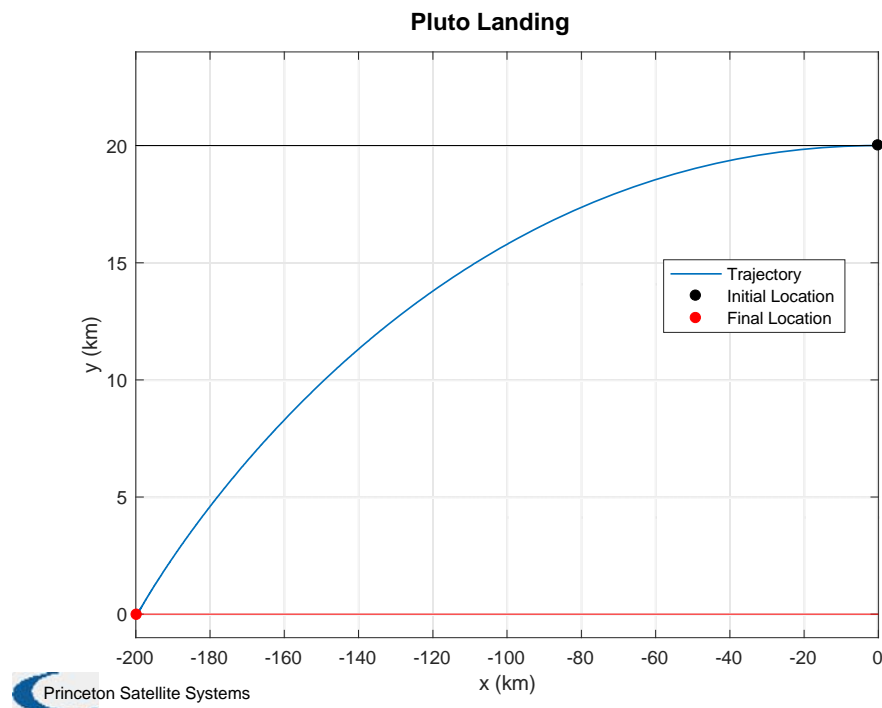
Figure 46. Pluto Landing Simulation using a Bilinear Tangent Law

Table 20 gives a rough mass budget for the lander. The battery was sized assuming a specific power of 200 Wh/kg.

Table 20 Lander Mass Budget

Subsystem/Component	Mass (kg)
ACS Subsystem	1.25
Propulsion Subsystem	90.9
Thruster	5
Fuel Tanks	6
Fuel	80
Telemetry and Command	1
Power Subsystem	26.63
Battery	13.3
Panels	13.2
Structure	23.69
Payload	86.55
TOTAL	230

4 Conclusions

Engine modeling accomplished during Phase I has shown that we can expect 2.5 to 5 N of thrust per megawatt of fusion power, with an Isp of about 10,000 seconds and 200 kW available as electrical power. We have evaluated the components of the Pluto trajectory including an Earth departure spiral, constant thrust planar transfer, and Pluto insertion using these thrust and Isp levels, and confirmed the plausibility of the proposed mission. In fact, the mission can depart from LEO with about the mass we originally estimated for an interplanetary insertion, widening the range of available launch vehicles and reducing the cost.

Our mass model analysis has identified those components which drive the engine mass, namely the superconducting magnets and the shielding. Using high-temperature superconductors is desired due to the reduced cost and complexity of liquid nitrogen cooling systems as compared to liquid helium needed for traditional low-temperature superconductors. However, first and even second-generation high-temperature superconductors have low engineering current densities due to substrates and metal classing swathing the strip of superconductor. This would result in masses too high for our target specific power. We have proposed further study in Phase II of the relationships between superconducting material, operating temperature, neutron tolerance, cooling system mass, and shielding mass, since these are interrelated.

Our analysis of the thermal conversion subsystem indicated reasonable component masses to support our system scaling laws. Our RF subsystem analysis did not proceed as far but we developed a new design for a much higher efficiency system using switching amplifiers. This is also proposed for further study.

In addition to preparing this final report, we have also prepared a draft design document for Direct Fusion Drive, which contains additional technical details of all the subsystems. This

document is design to serve as the basis for further design work and gathers all relevant technical information in a single place.

5 Bibliography

A. Bushman, D. M. Carpenter, T. S. Ellis, et. al. *The martian surface reactor: An advanced nuclear power station for manned extraterrestrial exploration.* . Technical Report, MIT, Nuclear Space Application Program , 2004.

Bingren, S. "Core Plasma Characteristics of a Spherical Torus Fusion Reactor." *Plasma Science & Technology* 7 (April 2005): 00.

Cohen, A. H. Glasser and S. A. "Ion and electron acceleration in the field-reversed configuration with an odd-parity rotating magnetic field." *Physics of Plasmas* 9, no. 5 (May 2002): 2093-2102.

Hively, L. *A Simple Computational Form for Maxwellian Reactivities.* Technical Note, Plasma Engineering, 1982.

Lewis, R. *Space shielding materials for Prometheus application.* Technical Report, Knolls Atomic Power Laboratory, 2006.

M. Eisterer, Michal Chudy, H. W. Weber. "Neutron irradiation of coated conductors." *Superconductor Science and Technology*, August 2009.

Mason, L.S. *A comparison of brayton and stirling space nuclear power systems for power levels from 1 kilowatt to 10 megawatts* . Technical Report, NASA Glenn Research Center , 2002.

Mason, Lee S. *Power Conversion Concept for the Jupiter Icy Moons Orbiter* . Technical Report, NASA Glenn Research Center, 2003.

R.W. Hyers, B.N. Tomboulian, P.D. Craven, and J.R. Rogers. *Lightweight, High-Temperature Radiator for Space Propulsion.* Presentation, Amherst: U. Mass Amherst, 2012.

S. A. Cohen, M. Chu-Cheong, R. Feder, K. Griffin, M. Khodak, J. Klabacha, E. Meier, S. Newbury, M. Paluszek, T. Roglien, S. Thomas, and M. Walsh. "Reducing Neutron Emission from Small Fusion Rocket Engines." *66th International Astronautical Congress.* Jerusalem: International Astronautical Federation, 2015. 7749-7750.

Santarius, J. F. *Generic Magnetic Fusion Rocket.* Technical Report, University of Wisconsin, 1998.

T.D. Rognlien, M.E Rensink, and G. R. Smith. *Users' Manual for the UEDGE Edge-Plasma Transport code.* N/A: LLNL, 2000.

6 Acronyms

APU – Auxiliary Power Unit
CAD – Computer-Aided Design
DFD – Direct Fusion Drive
DOE = Department of Energy
FRC – Field-Reversed Configuration
HTS – High-Temperature Superconductors

ITER - International Thermonuclear Experimental Reactor
LSP – Large Scale Plasma
LTS – Low-Temperature Superconductor
NRL – Naval Research Lab
PFRC - Princeton Field-Reversed Configuration
PPPL – Princeton Plasma Physics Lab
PSS – Princeton Satellite Systems
RMF – Rotating Magnetic Field
RF – Radio frequency
SOL – Scrape-off-layer

Appendix A.   PFRC Technical Description

This section provides a description of the PFRC that is intended for a general technical audience, without requiring plasma physics expertise. The interested reader is referred to our many physics publications for further details.

A.1   PFRC Overview

The Princeton Field Reversed Configuration (PFRC) nuclear fusion reactor is a revolutionary approach to fusion power generation. The reactor is small and clean, producing very few damaging neutrons and enabling rapid development at relatively low cost. The 1-10 MW reactors are suitable for diverse applications, from submarines to urban environments to space propulsion.

The PFRC plasma is confined in a magnetic torus inside of a linear solenoidal coil and is heated by a rotating magnetic field to fusion temperatures. The rotating field creates closed field lines, enclosed by an ellipsoidal separatrix. Ionized gas flows from the gas box on the left, along the separatrix in the cool scrape-off-layer, collecting energy from the fusion products as it goes. In a Direct Fusion Drive version of the engine, one or more nozzle coils on the right accelerate the ions and produce thrust. Heat from the neutrons and radiation losses is collected along the walls and converted to electrical power using a Brayton engine.
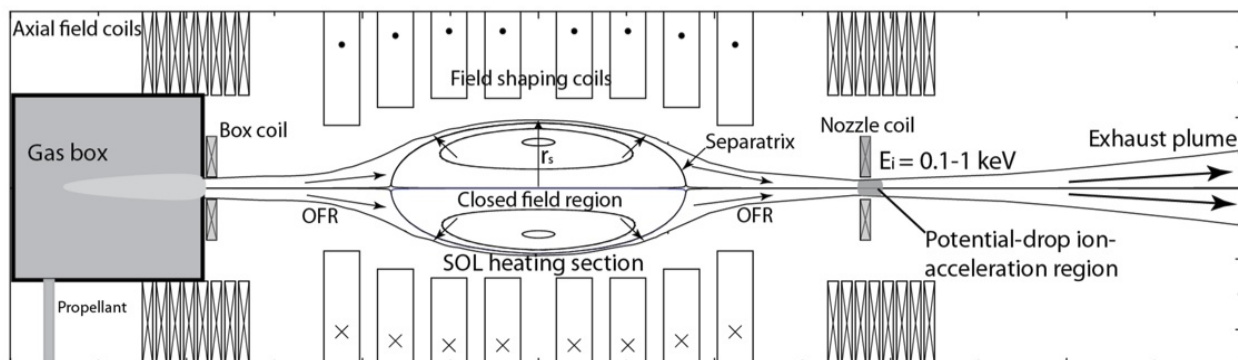
Figure 47. PFRC Schematic showing the magnetic field topology and locations of the coils

The rotating field is produced by external antenna perpendicular to the axis of the machine. The rotating field strength is about 1% of the strength of the axial field. The antennae are figured-8

shaped, with the direction of the induced field having opposite directions on either side of the machine midplane. This leads to the name, "odd-parity" heating, which contrasts with the traditional "even-parity" heating configuration. The odd configuration uniquely produces closed field lines of the internal torus. This method of heating was invented by PPPL scientist Dr. Sam Cohen.
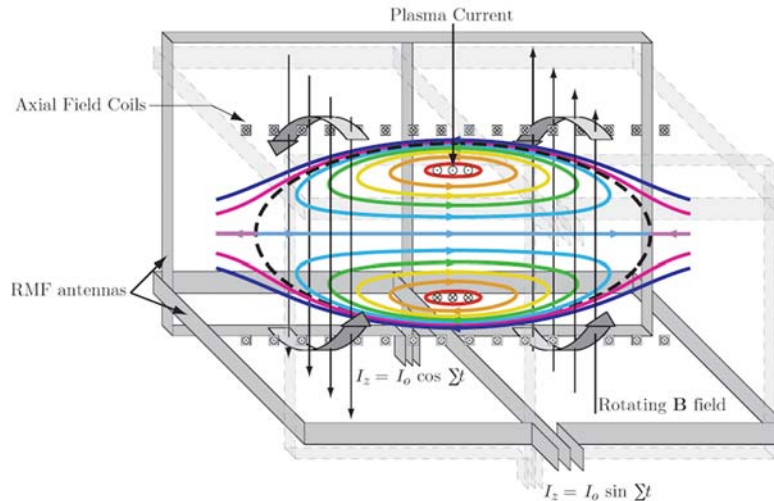
Figure 48. External antenna produce rotating magnetic fields. The azimuthally rotating electric field results in a plasma current.

The PFRC is designed to produce exceptionally few neutrons. The primary fuels are the deuterium and helium-3, which produce only charged particles and no neutrons. Deuterium-deuterium side reactions will produce small numbers of moderate energy neutrons and some tritium. If the tritium fuses with deuterium, high energy neutrons are produced which are very damaging. The small size of the machine facilitates the rapid exhaust of tritium ash thus eliminating these harmful deuterium-tritium side reactions. The production of neutrons is reduced further by altering the fuel ratio to have three times the helium-3 as deuterium, i.e. a ratio of 3:1, favoring the helium-3 reactions.

Competing fusion concepts such as tokamaks that burn deuterium-tritium fuel suffer from high production of very damaging neutrons. These machines require complex, expensive, and thick shielding systems. Power these gigawatt scale reactors must be extracted using 1 m-thick liquid lithium layers. The lithium itself is hazardous. Even with the lithium shielding, the irradiated reactor walls will need to be frequently replaced. The PFRC can be shielded simply with boron carbide, a chemically stable solid.

The field-reversed configuration results in a high beta, which is the ratio of the plasma pressure to the applied magnetic field. This allows for a high pressure to be achieved with a lower magnetic field. A tokamak has a beta of only 1-8% while the PFRC will have a beta approaching 1.

The simple geometry of the machine, low radiation, and moderate magnetic field strength all contribute to lowering development and maintenance costs. There are no hazardous fuels or materials required. The PFRC has been designed to be safe and affordable.

A.2   The Field-Reversed Configuration

The FRC is a closed magnetic field topology that is achieved without any central penetrations or magnets. This results in a compact toroid inside a cylindrical plasma. Plasma current flows in the toroid perpendicularly to the applied external field. The field in the center of the toroid is reversed with respect to the external field. This configuration may be achieved in a variety of ways; when formed using an inductive electric field (theta-pinch), the axial field is literally reversed around a pre-ionized gas. FRCs can also be formed, sustained, and heated by application of neutral beams.
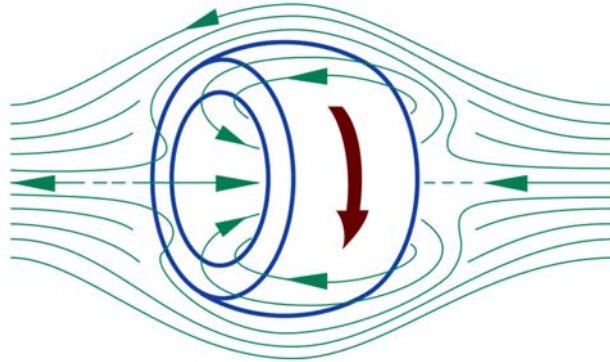
Figure 49. Field-Reversed Configuration. Credit: Wikimedia Commons

Rotating field methods using external coils are classified as even-parity or odd-parity. The rotating field is generated by external coils or antenna and the direction of this field is rotated about the machine axis. *When the rotation frequency is between the ion and electron gyro-frequencies, the electrons in the plasma co-rotate with the magnetic field (are "dragged"), producing current and reversing the magnetic field.*

FRCs contain an important and uncommon feature: a "magnetic null," or circular line on which the magnetic field is zero. Inside the null the magnetic field points in one direction and outside the null the magnetic field points the opposite direction. Particles far from the null trace closed cyclotron orbits as in other magnetic fusion geometries. Particles that cross the null, however, trace not cyclotron or circular orbits but betatron or figure-eight-like orbits, as the orbit's curvature changes direction when it crosses the magnetic null. Figure 50 shows an FRC particle trajectory in which a particle starts with cyclotron motion inside the null, transitions to betatron motion, and ends as cyclotron motion outside the null. This motion occurs in the mid-plane of the machine.
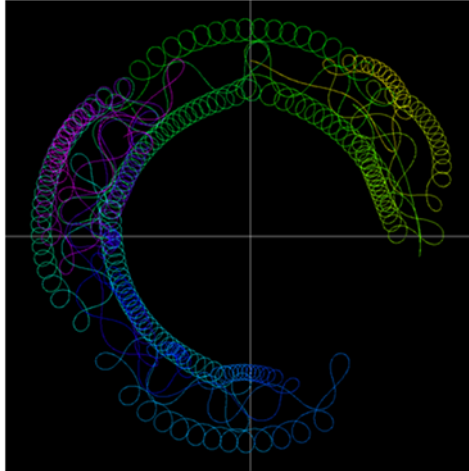
Figure 50. FRC particle trajectory in which a particle transitions from cyclotron motion to betatron motion and back. Credit: Wikimedia Commons

Because the particles orbits are not cyclotron, models of plasma behavior based on cyclotron motion like Magnetohydrodynamics (MHD) are entirely inapplicable in the region around the null. The size of this region is related to the s-parameter, or the ratio of the distance between the null and separatrix, and the thermal ion gyroradius. This is the number of ion orbits that can fit between the core of the FRC and where it meets the cool bulk plasma. At high-s, most particles do not cross the null and this betatron effect is negligible. At low-s, about 2, this effect dominates and the FRC is said to be "kinetic" rather than "MHD."

The PFRC fuel will have an *s*-parameter of about 10 while the fusion products will have an *s*-parameter between 1 and 3.

A.3   PFRC Fusion Reactions

There are four fusion reactions of interest for a deuterium/helium-3 reactor. The first is the deuterium/helium-3 reaction itself, which produces no neutrons. There are two deuterium-deuterium side reactions, which will occur in nearly equal proportions. One of these produces a moderate energy neutron and more helium-3 while the other produces tritium and a proton. The final reaction, deuterium-tritium, produces a dangerous high-energy neutron.

$D + {}^3He >$ He (3.6 MeV)   + p (14.7 MeV)
$D + D >$ T (1.01 MeV)   + p (3.02 MeV)
$D + D >$ ${}^3He$ (0.82 MeV)   + n (2.45 MeV)
$D + T >$ He (3.45 MeV)   + n (14.1 MeV)

Figure 51 shows the cross-sections of the relevant fusion reactions. The D-He3 reaction rate is considerably higher that the D-D reaction rate at the target temperature of 100 keV. Note that the D-T cross section is even higher than D-He3 at this temperature, which makes removing the tritium critical.
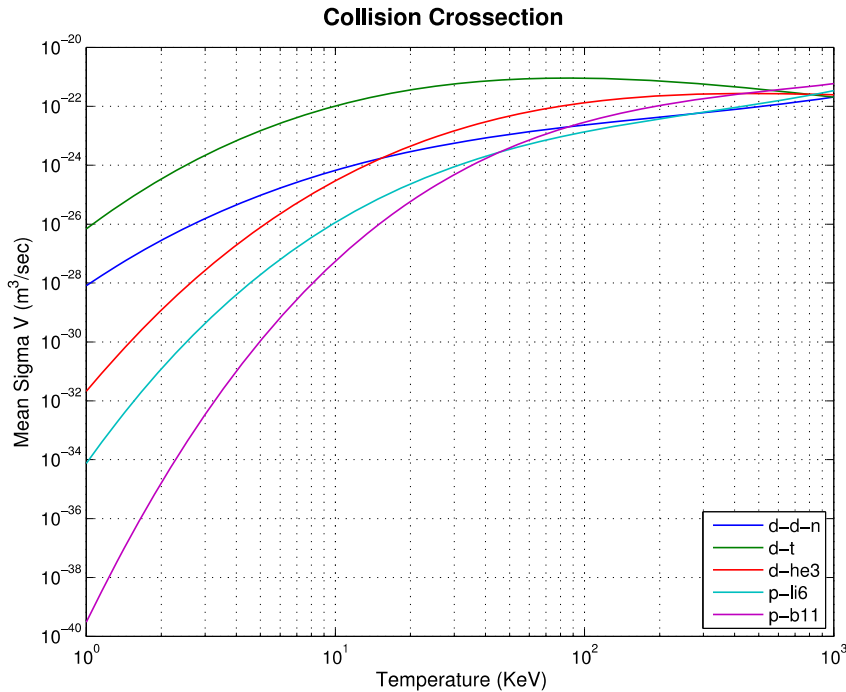
Figure 51 Fusion Reaction Cross Sections.

In the PFRC, about 99% of the power is projected to be in the D-^{3}He reactions, and about 0.5% in each of the deuterium-deuterium reactions. The tritium is exhausted before it can fuse, so that the power in that reaction should approach zero.

A.4   RMF Heating Method

For an FRC reactor to burn a D – ^{3}He fuel mixture, the plasma ions must be heated to over 50 keV. If energetic neutral-beam injection were used for achieving these temperatures, the plasma would have to be over 4 m in diameter in order to "stop" the injected neutral beam. Such a large reactor would produce proportionally large amounts of power, near 1 GW. In RF heating methods, on the other hand, power can be absorbed over shorter distances. Using odd-parity RMF allows the diameter of the plasma to be reduced to 0.5 m and produce 1 MW.

In odd-parity RMF heating, the maximum ion energy is proportional to the RMF frequency ω_{RMF}. Due to a constraint set by the RMF-generated current and the FRC's magnetic field strength, the RMF frequency decreases as the product of plasma density times the square of the plasma radius. Thus, too large or dense an FRC is not well heated. An optimum FRC for RMF heating of ions to 100 keV and above has a radius in the range from 20 to 30 cm.

RMF creates a time-varying azimuthal electric field near the O-point null line [Glasser, 2002]. This periodically accelerates ions into betatron orbits and then decelerates them back into cyclotron orbits. Choosing the frequency and amplitude properly allows ions to be pumped up, repeatedly, to energies near the peak of the D–^{3}He fusion cross-section and then returned to the bulk temperature. In a D–^{3}He plasma, the trajectories of the accelerated ions are predicted to form two betatron-orbit streams close to the FRC's O-point null line, a D stream and a ^{3}He

stream. The deuterium stream ions have half the peak energy of the ^{3}He ions, causing non-zero relative velocity between them. The energy dependent fusion rates can be used to show the basic effect of the higher energy of the ^{3}He stream. If the bulk plasma has an average energy of 70 keV and the RMF pumps the ^{3}He up by 100 keV it will pump the deuterium up by only 50 keV. This favors the desirable D-^{3}He reactions and reduces the percentage of fusion power in deuterium-deuterium reactions, to less than 1%.
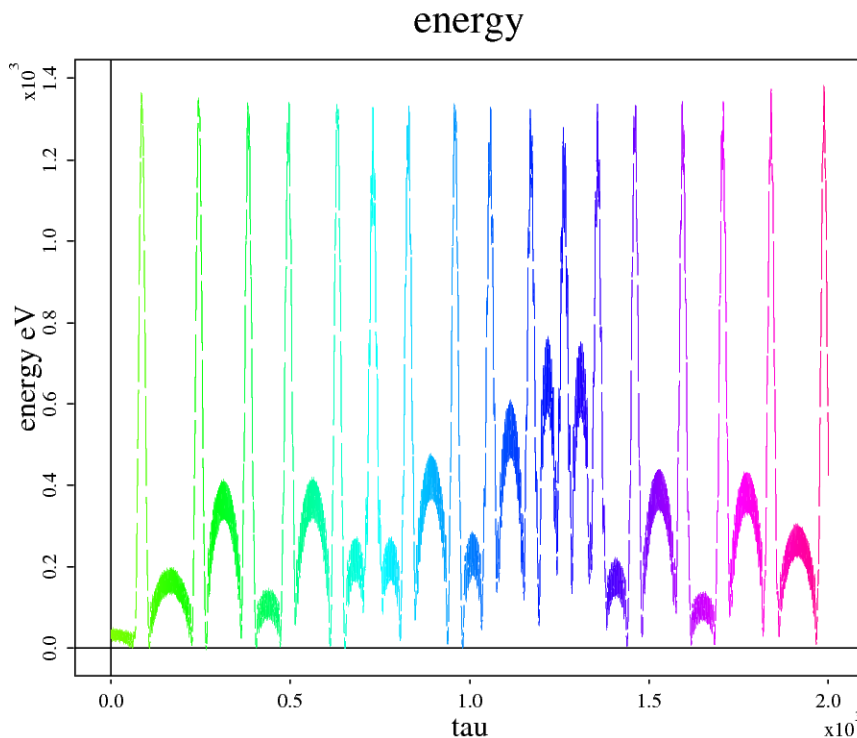
energy

Figure 52 Ion Trajectories showing energy pumping (RMF Software)

A.5 Reduction of Neutrons

Overall, the shielding requirements for this type of small, clean reactor are far less than for a larger deuterium-tritium fusion engine. The neutrons from the D-D side reactions are only 2.45 MeV, which is 1/6 of the energy of those produced by D–T. The larger surface-to-volume ratio for a small FRC, about 25 cm radius, compared to a large tokamak, about 10 m, results in a 200-fold reduction in neutron power load on the wall.

With a low s value of around 3, the energetic tritium products will pass across the separatrix and traverse the cold scrape-off-layer. The tritium products slow down in about 0.01 s while the characteristic burn-up time is 20 s. Their trajectories end up fully in the SOL, from where they are promptly expelled with the propellant.

A.6 Radiation Losses

There are two key mechanisms for radiation loss from the plasma: synchrotron radiation and bremsstrahlung. Synchrotron is produced due to the acceleration of ultra-relativistic charged

particles through magnetic fields. Since we are confining the plasma with magnetic fields we will always get synchrotron radiation. Bremsstrahlung or "braking radiation" is due to the deceleration of a charged particle when deflected by another charged particle, typically an electron by an atomic nucleus. Since our plasma is a mix of electrons and nuclei this will happen frequently. Both types of radiation are electromagnetic.

Heat from the radiation losses is converted to electrical power using a thermal conversion system. A Brayton engine can be up to 60% efficient.

A.7   Thrust Augmentation

Thrust augmentation is the process by which additional ionized gas flows through the PFRC and produces thrust. The fusion products alone, if ejected directly from the engine, would have a velocity of 25,000 km/s and produce negligible thrust. In the PFRC, these products interact with cool ionized gas in a region called the scrape-off-layer (SOL). Energy is transferred from the hot products to the SOL electrons, and this energy is in turn transferred to the ions in the magnetic nozzle. The result is an exhaust with a bulk exist velocity of about 100 km/s and a thrust of about 2.5 to 5 N per MW of fusion power.

The magnetic nozzle has been studied under separate DOE grants for the Magnetic Nozzle Experiment (MNX) program. The LPS particle-in-cell code has been used to study plasma detachment. Figure 53 shows an example result for ion kinetic energy at 3110 nanoseconds. Figure 54 shows the ratio of the axial velocity fraction to the axial magnetic field fraction, indicating values higher than one. These studies verify that electron energy is transferred to the ions and that detachment from the magnetic field lines occurs.
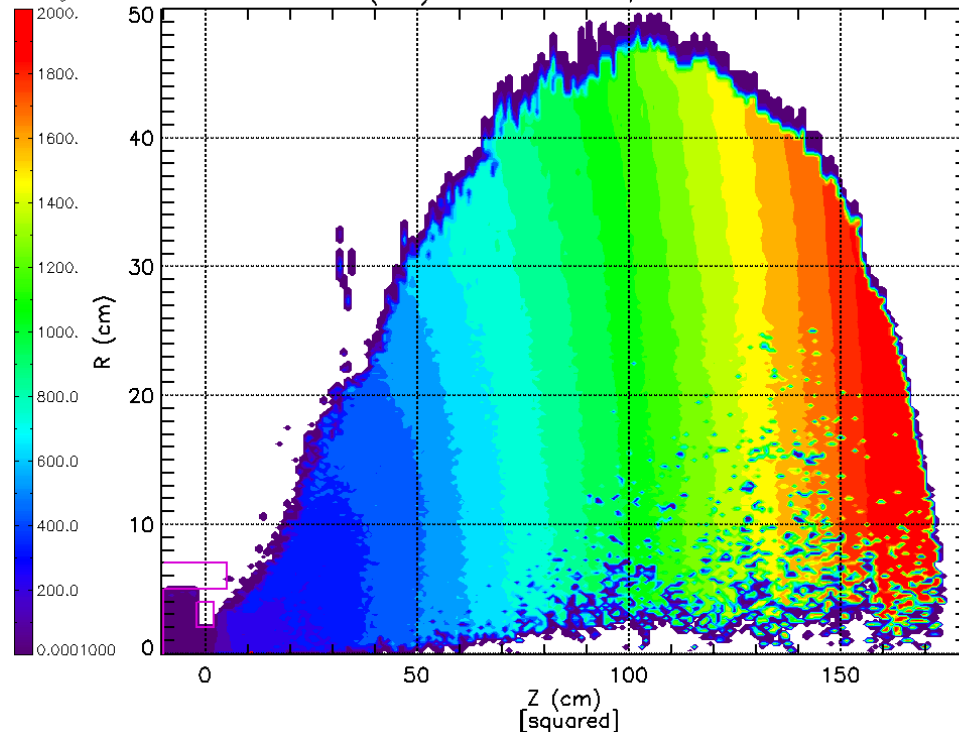
Figure 53. Ion Kinetic Energy from LSP PIC Simulation
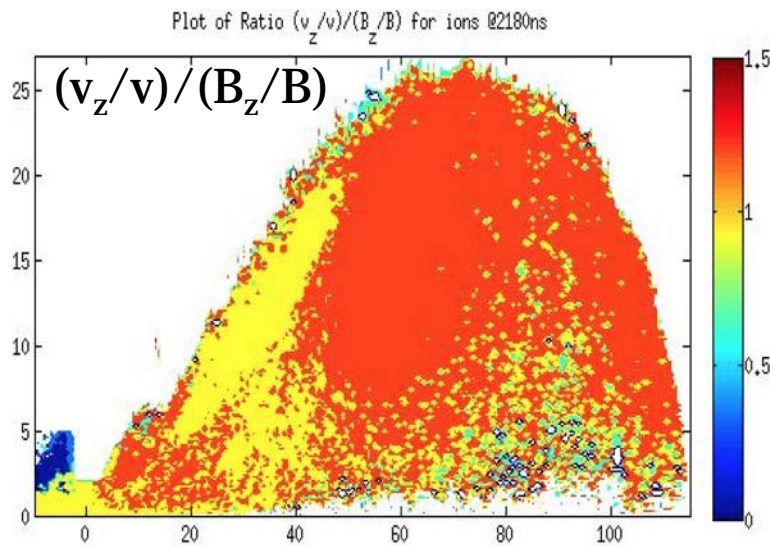
Figure 54. Ratio of Axial Velocity Component to Axial Field Component from LSP PIC Simulation

A.8   Development Plan

PPPL is developing PFRC-2 with a grant from DOE. PFRC-2 will characterize ion heating and PFRC-3 would achieve fusion power generation. Each stage of this phased development plan, Figure 55, is designed to reach significant scientific and technological milestones. When the scientific objectives of PFRC-3A have been met, the fuels will be changed so that fusion power production and energy and ash extraction techniques can be demonstrated in PFRC-3B.

Machine	PFRC−1	PFRC−2	PFRC−3A	PFRC−3B
Objectives	Electron Heating	Ion Heating	Heating above 5 keV	D−He3 Fusion
Fuel	H	H	H	D−3He
Goals/Achievements*	3 ms pulse* 0.15 kG field* e−temp = 0.3 keV*	0.1 s pulse* 1.2 kG field i−temp = 1 keV	10 s pulse 10 kG field i−temp = 5 keV	10 s pulse 80 kG field i−temp = 50 keV
Plasma Radius	4 cm	8 cm	16 cm	16 cm
Time Frame	2008−2011	2011−2015	2015−2019	2019−2020
Total Cost	$2M	$6M	$20M	$20M

Figure 55. PFRC Development plan

The next sections further describe the experimental stages. Following PFRC-3B, the next step would be a full-scale PFRC-4 reactor with a plasma radius of 25 cm.

PFRC-2: Prove ion heating method
The goal of PFRC-2 is to achieve 0.1-second-duration hydrogen plasmas with 1-keV ion and electron temperatures at a magnetic field strength of 1.2 kG. Plasmas of this temperature have never before been made in FRCs. When such temperatures were achieved in tokamak research nearly 50 years ago, international fusion research rapidly grew. The main technical achievements for the PFRC-2 have been the implementation of an array of passive high-temperature

superconducting (HTS) magnets and construction of a higher power RF plasma heating system, with antennae external to the vacuum vessel. This plasma heating system would be useful for other applications, e.g., semiconductor/materials processing and spacecraft propulsion.

PFRC-3A: Achieve thermonuclear parameters

The goal is to increase the pulse length to 10 seconds, the temperature to 5 keV, and the magnetic field to 10-kG magnetic field. The plasma parameters achieved would be adequate for D-T fusion though not for *really clean* (D-^{3}He) fusion. This high power, near steady-state plasma source could be useful for many applications, including toxic waste destruction and heat flux generation for materials fabrication and testing.

- A full array of active HTS magnets would be designed, prototyped, built, and tested. These will allow sufficiently long pulses that most steady-state heat-load questions can be answered.
- Additional diagnostics and a higher power RF system would be built and installed.
- First tests of the thrust augmentation and efficient ^{3}He fueling methods would be made.
- Scenarios for stage 3B would be developed. These include studies of energy confinement and (current-drive efficiency. (

PFRC-3B: Demonstrate low-neutron-production fusion and ash- and energy-removal methods

The goal is to achieve 100-minute total operation of 100-second-duration D-^{3}He plasmas with fusion demonstrated at $0.1 < Q < 2$. The ion temperature would need to reach 50 keV and the magnetic field 60 kG.

- Neutron shielding would be added.
- Neutron and Q diagnostics would be added.
- This stage would use the same full HTS magnet array as 3A, except the field would be raised a factor of 6, about 1/4th of the current limit for HTS.
- Operational scenarios for efficient ^{3}He fueling, novel energy extraction methods, and fusion power control would be developed.
- Modeling of He-catalyzed D-D fusion for terrestrial power generation will be made, guided by the experimental results.

A.9   PFRC Summary

A PFRC reactor would be about 2 m in diameter, 10 m in length, and produce between 1 and 10 MW of steady-state fusion power. The novel radio-frequency plasma heating system enables the achievement of sufficiently high plasma temperatures for deuterium-Helium 3 fusion. The size of the machine and the operational fuel ratio combine to dramatically lower the neutron wall load compared to traditional deuterium-tritium machines. The machine requires no radioactive or dangerous materials and requires only modest amounts of shielding for safe operation.
The low radioactivity and simple geometry reduce the development costs dramatically as compared to other fusion concepts. We estimate that PFRC-3A and PFRC-3B can be completed for about $50MM and five to ten years, depending on the funding profile.